Published in final edited form as:

Langmuir. 2021 August 03; 37(30): 9120–9136. doi:10.1021/acs.langmuir.1c01204.

Bacterial Quorum Sensing Signals Promote Large-Scale Remodeling of Lipid Membranes

Curran G. Gahan[1], **Samarthaben J. Patel**[1], **Lawrence M. Chen**[1], **Daniel E. Manson**[2], **Zachary J. Ehmer**[1], **Helen E. Blackwell**[2], **Reid C. Van Lehn**[1], **David M. Lynn**[1,2]

[1]Dept. of Chemical and Biological Engineering, Univ. of Wisconsin–Madison, 1415 Engineering Dr., Madison, WI 53706

[2]Dept. of Chemistry, Univ. of Wisconsin–Madison, 1101 University Ave., Madison, WI 53706, USA

Abstract

We report that *N*-acyl-L-homoserine lactones (AHLs), a class of nonionic amphiphiles that common bacteria use as signals to coordinate group behaviors, can promote large-scale remodeling in model lipid membranes. Characterization of supported lipid bilayers (SLBs) of the phospholipid DOPC by fluorescence microscopy and quartz crystal microbalance with dissipation (QCM-D) reveals the well-studied AHL signal 3-oxo-C12-AHL and its anionic head group hydrolysis product (3-oxo-C12-HS) to promote the formation of long microtubules that can retract into hemispherical caps on the surface of the bilayer. These transformations are dynamic, reversible, and dependent upon head group structure. Additional experiments demonstrate that 3-oxo-C12-AHL can promote remodeling to form microtubules in lipid vesicles and promote molecular transport across bilayers. Molecular dynamics (MD) simulations predict differences in thermodynamic barriers to translocation of these amphiphiles across a bilayer that are reflected in both the type and extent of reformation and associated dynamics. Our experimental observations can thus be interpreted in terms of accumulation and relief of asymmetric stresses in the inner and outer leaflets of a bilayer upon intercalation and translocation of these amphiphiles. Finally, experiments on *Pseudomonas aeruginosa*, a pathogen that uses 3-oxo-C12-AHL for cell-to-cell signaling, demonstrate that 3-oxo-C12-AHL and 3-oxo-C12-HS can promote membrane remodeling at biologically relevant concentrations and in the absence of other biosurfactants, such as rhamnolipid, that are produced at high population densities. Overall, these results have implications for the roles that 3-oxo-C12-AHL and its hydrolysis product may play in not only mediating intra-species bacterial communication, but also processes such as inter-species signaling and bacterial control of host-cell response. Our findings also provide guidance that could prove useful for the design of synthetic self-assembled materials that respond to bacteria in ways that are useful in the context of sensing, drug delivery, and in other fundamental and applied areas.

Graphical Abstract

(H.E.B.) blackwell@chem.wisc.edu; (R.C.V.) vanlehn@wisc.edu; (D.M.L.) dlynn@engr.wisc.edu.

Supporting Information. Additional plots, images, and videos providing qualitative and quantitative characterization and additional associated discussion of bilayer remodeling promoted by bacterial amphiphiles (PDF). This material is available free of charge via the Internet.

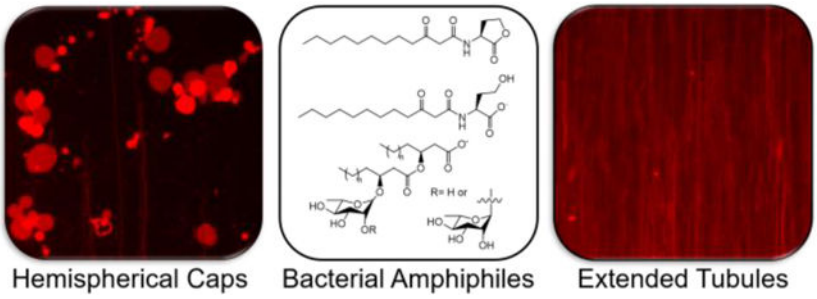

Introduction

Self-assembled lipid membranes are dynamic systems that respond to a variety of environmental stimuli, including changes in pH,[1,2] ionic strength,[3,4] and temperature,[1,5] through molecular reorganization,[6,7] phase changes,[5,8] and pore formation.[9,10] This dynamic behavior is central to life processes and has been exploited for the design of synthetic materials platforms for drug delivery, environmental sensing, separations, and in many other fundamental and applied contexts.[1,11–14] Both natural and synthetic lipid membranes can undergo structural transformations in the presence of molecules in their environment, including amphiphilic species that can adsorb to, intercalate into, or translocate across their inner and outer leaflets.[15,16] In this study, we report on large-scale remodeling of model synthetic lipid membranes promoted by contact with *N*-acyl-L-homoserine lactones (AHLs), a class of nonionic, small-molecule amphiphiles that species of Gram-negative bacteria use as intercellular signals to coordinate group behaviors,[17–19] including motility,[20] the production of sessile drug-resilient biofilms,[21,22] and the synthesis of virulence factors such as the biosurfactant rhamnolipid.[23] This signaling process is called quorum sensing (QS) and is widespread in common bacterial pathogens.

Of particular interest to the work described here are past reports demonstrating that AHLs, which possess a relatively polar L-homoserine lactone “head group” and an aliphatic “tail” of four to 20 carbons (Figure 1), can self-assemble in aqueous solution and at interfaces.[24–26] For example, past work by our group[26] and others[25] has demonstrated that long-chained AHLs (e.g., those possessing eight or more carbons in their tails) can self-assemble in solution to form spherical micelles or small (~20 nm) vesicles in a tail-length dependent manner. Daniels *et al.* have also demonstrated that AHLs can self-assemble and undergo phase changes when compressed at air-water interfaces.[24] Other groups have reported that AHLs are able to intercalate via their tails into the hydrophobic core of a lipid membrane,[27–29] leading to changes in a variety of membrane properties, including membrane depolarization[30] and the dissolution of lipid rafts.[31] Finally, studies by Lentini et al. have also, in the cases of 3-oxo-C8-AHL and the short-chained AHLs C4-AHL and 3-oxo-C6-AHL, demonstrated their translocation across model lipid bilayer systems.[32] These results are significant because, when combined, they hint at roles that these amphiphilic signaling molecules may play beyond their widely studied roles as mediators of bacterial cell-cell communication. For example, the ability of these molecules to self-assemble at or within lipid membranes may help facilitate the transport of these signaling molecules between bacterial cells,[29] attenuate their activity profiles, and could potentially underlie

mechanisms by which communities of bacteria influence interspecies signaling, host-cell behavior, or even engage in interkingdom signaling.[33,34] More broadly, the ability of AHLs to interact with lipid membranes suggests the potential to design synthetic materials that interact dynamically with bacterial communities.[32,35]

In this study, we demonstrate that 3-oxo-C12-AHL (Figure 1), an AHL with a 12-carbon tail produced by the opportunistic pathogen *Pseudomonas aeruginosa* and related bacteria, can interact with model supported lipid membranes (SLBs) in ways that promote large-scale remodeling. Characterization by fluorescence microscopy and quartz crystal microbalance with dissipation (QCM-D) reveal the formation of extended tubule structures up to hundreds of microns in length, as well as hemispherical caps that form on the surface of 1,2-dioleoyl-sn-glycero-3-phosphocholine (DOPC) lipid membranes upon exposure to solutions of 3-oxo-C12-AHL and its anionic head group hydrolysis product 3-oxo-C12-HS.[36] The nature and extent of remodeling is dependent upon the chemical structures of these amphiphiles and is at least partially reversible. These experimental observations can be interpreted in view of molecular dynamics (MD) simulations of thermodynamic barriers to translocation for 3-oxo-C12-AHL and 3-oxo-C12-HS. These simulations provide a theoretical framework for interpreting lipid remodeling in terms of differences in the intercalation and translocation of these compounds in the inner and outer leaflets of a lipid membrane. This framework also permits comparisons to the results of other past studies on the interaction of natural and synthetic amphiphiles with SLBs.[37] Finally, experiments using culture supernatants of wild-type *P. aeruginosa* and a related mutant strain demonstrate that 3-oxo-C12-AHL and 3-oxo-C12-HS can promote membrane remodeling at biologically relevant concentrations and in the absence of other biosurfactants (e.g., rhamnolipid) produced at high cell densities. These results provide insight into the potential roles that 3-oxo-C12-AHL and 3-oxo-C12-HS may play in bacterial communities, including QS mechanisms and potential mechanisms for interactions with non-self bacteria and their host organisms. Additionally, the results of these studies with model lipid membranes provide guidance that could advance an important long-term goal—understanding the range of interactions that can occur between bacterial communities and synthetic self-assembled materials—thereby providing new principles for the development of responsive materials for drug delivery and sensing applications.

Materials and Methods

Materials.

Dimethylsulfoxide (DMSO), sodium chloride (NaCl), calcein, sodium hydroxide (NaOH), lithium hydroxide (LiOH), magnesium sulphate, acetone, triethylphosphine oxide, Sephadex G-50, white, light mineral oil, and deuterium oxide (D_2O) were obtained from Sigma (St. Louis, MO). 1,2-Dioleoyl-sn-glycero-3-phosphocholine (DOPC) and 1,2-dihexanoyl-sn-glycero-3-phosphocholine (DHPC), L-α-phosphatidylglycerol (Egg PG), filter supports, and a Mini-prep extruder were purchased from Avanti Polar Lipids (Alabaster, AL). Lissamine rhodamine B 1,2-dipalmitoyl-sn-glycero-3-phosphoethanolamine, triethylammonium salt (Rho-DPPE) was acquired from Invitrogen (Carlsbad, CA). Rhamnolipids, 90% pure (commercial mixture of glycolipids isolated from *P. aeruginosa*) were purchased from AGAE Technologies (Corvallis, OR). Lennox formulation Luria-Bertani (LB) medium

powder from Research Products International (Mt. Prospect, IL) was used for bacterial culture. Electrophoresis-grade sodium dodecyl sulfate (SDS) was purchased from Fisher Scientific (Pittsburgh, PA). Triton-X100 was obtained from Promega (Madison, WI). MOPS was purchased from MP Biomedical (Irvine, CA). Minisort X plus 0.2 μm syringe filters were acquired from Sartorius Stedim Biotech (Goettingen, Germany). Isopropanol (iPrOH) was purchased from Fisher Scientific (Waltham, MA). 100 nm polycarbonate extruder filters were purchased from Millipore (Billerica, MA). Water was purified using a Milli-Q system (Millipore, Bedford, MA), yielding water with a resistivity of 18.2 MΩ. All materials were used as received without further purification unless otherwise specified.

Synthesis of 3-oxo-C12-AHL and 3-oxo-C12-HS.

3-oxo-C12-AHL was synthesized using a procedure previously described in the literature and matched the reported NMR spectra.[38] To synthesize 3-oxo-C12-HS, 3-oxo-C12-AHL (73 mg, 0.25 mmol) was added to a glass vial equipped with a stir bar and dissolved in acetone (1 mL). Aqueous lithium hydroxide (10 drops of 1M solution) was added to the vial, and the reaction was stirred at room temperature. Reaction progress was monitored by thin layer chromatography. Upon consumption of starting material, the reaction mixture was dried with magnesium sulfate, filtered, and concentrated under reduced pressure to yield 3-oxo-C12-HS as a white solid. NMR spectra are provided for 3-oxo-C12-HS in the Supporting Information.

Cell Culture and Supernatant Collection.

The *P. aeruginosa* strains used in this study were: PAO1 (wild-type)[39] and PW6886 (*ΔrhlA*) (PAO1 *rhlA-E08::ISphoA/hah*; tetracycline resistant).[40] All strains were cultured in LB medium. Freezer stocks of each strain were streaked on an LB agar plate and allowed to grow overnight at 37 °C. Single colonies were then placed into 2 mL of fresh LB medium and allowed to grow overnight. Aliquots (30 μL) of these overnight cultures were diluted into 3 mL of fresh LB medium in 16 × 100 mm culture tubes and grown at 37 °C with shaking at 200 rpm. At designated timepoints, the cultures were aliquoted into 1.7 mL centrifuge tubes and centrifuged at 16,000 g for 5 minutes to pelletize the cells. The culture supernatants were isolated and passed through a sterile 0.22 μm filter. Supernatants were immediately frozen and then thawed directly before use.

Preparation of Biosurfactant Solutions.

Stock solutions of rhamnolipid in buffer (1 mg/mL) were made fresh before each experiment. A buffer solution of 150 mM NaCl, 10 mM MOPS in Milli-Q H_2O (pH 7.4) was used unless otherwise noted. All aqueous solutions used in this study contained 1 vol% DMSO, except for bacterial supernatants and LB medium. The rhamnolipid stock solution was sonicated briefly to assist in dissolution. To make rhamnolipid solutions of the desired concentration, the stock solution was diluted with additional buffer. Stock solutions of 3-oxo-C12-AHL and 3-oxo-C12-HS (20 mM) were made in DMSO and stored at −4 °C between uses. Aliquots of the stock solution were thawed immediately prior to experiments. To prepare aqueous AHL solutions, the stock solutions were first diluted in DMSO to 100 times the final aqueous concentration, and then diluted 1:100 into buffer or a solution containing rhamnolipid. All AHL solutions were used within 1 hour of their preparation

to minimize changes in the ratios of hydrolyzed and unhydrolyzed AHL head groups in solution.

Vesicle Fabrication.

All large unilamellar vesicles (LUVs) were prepared using a freeze-thaw and vesicle extrusion procedure.[41] In brief, desired amounts of DOPC dissolved in chloroform were aliquoted into vials, and the chloroform was removed under a stream of N_2. For fluorescence microscopy experiments, 0.1 wt% of fluorescently labeled lipid (Rho-DPPE) was added to the chloroform stock solutions prior to drying under N_2. The lipids were further dried under vacuum for at least an hour. Either fresh LB medium (for supernatant experiments) or a low salt buffer solution (10 mM NaCl and 10 mM MOPS in water; for controlled biosurfactant experiments) was added to the dried lipids and vortexed vigorously to form a turbid 5 mg/mL DOPC suspension. These vesicle solutions were then subsequently frozen and thawed five times by alternatively immersing them into an iPrOH/dry ice bath and a warm water bath (~50 °C). The resulting vesicle suspension was passed at least 11 times through a 100 nm PC filter using an Avanti Polar Lipids Mini-prep extruder. The resulting vesicles were characterized by dynamic light scattering (DLS) (Malvern Zetasizer, Westborough MA) and found to have a hydrodynamic diameter of ~140 nm, which agrees with previously reported literature.[42]

To prepare calcein-loaded vesicles for dye leakage experiments, the dried lipid solution was hydrated with a solution of calcein (70 mM) in buffer. The pH of the solution was adjusted to 7.4 with 10 M NaOH. After five freeze-thaw cycles and extrusion, the vesicles were separated from external, unloaded calcein using a hand-packed Sephadex G-50 size exclusion chromatography column. The concentration of the resulting purified vesicle solution was then quantified using ^{31}P NMR as described in the Supporting Information.[43]

Giant Unilamellar Vesicle (GUV) Fabrication and Imaging.

GUVs were fabricated using a previously described inverted-emulsion protocol.[44] Briefly, a 99:1 ratio of DOPC:Egg PG (5 mg total) was mixed in chloroform with 0.1 wt% of the fluorescently labeled lipid Rho-DPPE and dried under a stream of N_2. The lipid was further dried under vacuum for at least an hour to remove residual solvent. This dried lipid mixture was then dissolved in mineral oil (1 mL). Buffer (40.5 μL) was added to 450 μL of the lipid-oil mixture and vortexed for 30 seconds to form a water-in-oil emulsion. A 450 μL aliquot of this emulsion was gently placed on top of buffer solution (450 μL) in a microcentrifuge tube and centrifuged for 30 minutes at 14,000*g*. After centrifugation, the lower aqueous phase (which contained the fabricated GUVs) was isolated and diluted into either an equal volume of buffer or a concentrated solution of 3-oxo-C12-AHL or rhamnolipid. This dilution resulted in a suspension of GUVs in either buffer, 100 μM of 3-oxo-C12-AHL, or 25 μg/mL of rhamnolipid for observation via optical microscopy. Only GUVs with a diameter greater than 15 μm were considered for investigation. We sorted each of the vesicles observed into two categories, those with external tubulation and those without. The proportions of vesicles in each group were calculated for three independent samples.

Optical Microscopy Experiments Using SLBs Formed by Vesicle Fusion Technique.

Fluorescence microscopy experiments were performed on fluorescently labeled SLBs that were formed using the vesicle fusion (VF) technique in Ibidi microfluidic chambers (μ-Slide VI 0.5 Glass Bottom) unless otherwise noted.[45] The microfluidic chambers first were cleaned with a 1 M NaOH aqueous solution for ~30 minutes prior to SLB formation, and then washed with ample Milli-Q H_2O followed by either LB medium (for supernatant experiments) or buffer (for biosurfactant experiments). Previously prepared LUV stock solutions (5 mg/mL) were diluted with buffer to 0.1 mg/mL and introduced to the cleaned microfluidic chambers at a flow rate of 100 μL/min using a NE-300 “Just Infusion” syringe pump (Coral Springs, FL). The formation of the bilayer was monitored by microscopy to ensure the adsorption and subsequent fusion of LUVs into a SLB as seen in Supporting Information Video S1. When fusion was verified, the remaining vesicles in the flow cell were washed away by introducing LB medium or buffer to the flow cell at a flow rate of 100 μL/min. The resulting bilayer was tested for fluidity by performing a qualitative fluorescence recovery after photobleaching (FRAP) experiment (Video S2). In initial control experiments, these SLBs responded to the presence of the amphiphile glycerol monolaurate (GML) in ways similar to those reported in past studies on the remodeling of DOPC membranes (Video S3; see previous reports by Cho and coworkers[37]). Cell-free culture supernatants or solutions of test compounds were introduced into flow cells at a flow rate of 100 μL/min, and micrographs were acquired using an Olympus IX70 inverted microscope (Center Valley, PA) and a Q-imaging EXi Aqua camera (Tucson, AZ) every 5 seconds for ~8 minutes (acquiring at least 100 images). Fluorescently-labeled lipids were excited with a Lumen Dynamics X-Cite Series 120PC-Q fiber coupled mercury lamp using the RFP channel (Monroe, LA). The bilayers were then washed with buffer solution at a flow rate of 100 μL/min to visualize changes in the bilayer structure as the test compounds were removed from solution.

Formation of DOPC SLBs Using the Bicelle Fusion Method.

As a second means of preparing SLBs, we used a previously described bicelle formation technique.[46] In brief, DOPC and DHPC ([DOPC]/[DHPC]=0.25) were dissolved in chloroform, the solution was well mixed, and solvent was removed under a stream of N_2 and then under vacuum for at least one hour. The resulting lipid film was then hydrated by buffer to produce a 1 mM bicelle suspension by DOPC concentration. This solution was frozen and thawed five times by iteratively immersing the solution into an iPrOH and dry ice bath followed by a warm water bath (~50 °C). The bicelle stock solution was then diluted 1:16 for a final DOPC concentration of 0.063 mM and introduced to an NaOH treated Ibidi flow cell at a flow rate of 100 μL/min. The formation of a continuous bilayer was monitored by optical microscopy (Video S4). Buffer was then introduced to the bilayer to wash away any remaining bicelle above the bilayer. The resulting bilayer was tested for fluidity by preforming a qualitative FRAP experiment (Video S5). Test compounds were then introduced into the flow cell at a constant concentration at a flow rate of 100 μL/min. Time-lapse micrographs were acquired every 5 seconds over ~8 minutes. The bilayers were then washed with buffer solution at a flow rate of 100 μL/min to visualize changes in bilayer structure as the test compounds were removed from solution.

Measurement of the Surface Tensions of Biosurfactant Solutions.

Measurements of the surface tensions of 3-oxo-C12-AHL, 3-oxo-C12-HS, and rhamnolipid solutions were made by adapting a previously described procedure.[47] The surface tensions of the biosurfactant solutions was measured using a Nima Type 611 trough. The tensiometer was calibrated using an internal calibration program and checked by ensuring the surface tension of Milli-Q water was near 72 mN/m. A dry paper Wilhelmy plate was immersed in Milli-Q water for 10 minutes at room temperature to hydrate before surface tension measurements were made. Biosurfactant solutions were prepared in buffer as described above and allowed to sit at room temperature, and then the hydrated Wilhelmy plate was dipped into the biosurfactant solution and allowed to sit at the solution interface for 30 seconds. The surface tension (γ) was determined by measuring the change in force applied to the Wilhelmy plate by the solution while in contact with the solution interface and directly after removing the plate from solution. This change in force (F) was then used in the Wilhelmy equation,[47]

$$\gamma = \frac{F}{l\cos(\theta)} \quad (1)$$

where l is the wetted perimeter of the paper Wilhelmy plate (21 mm) and θ is the contact angle of water on the Wilhelmy plate, which is assumed to be 0º for a paper plate.

Quartz Crystal Microbalance with Dissipation (QCM-D) Measurements.

QCM-D measurements were preformed using a Q-Sense E4 instrument (Bolin Scientific, Stockholm Sweden) with QSensor QSX 303 quartz crystal sensors coated with 50 nm of SiO_2 and with a fundamental frequency of 5 MHz (Bolin Scientific, Stockholm Sweden). Changes in the frequency (Δf) and dissipation (ΔD) were monitored at the third, fifth, seventh, ninth, and eleventh overtones, and data analysis was preformed using the data from the seventh overtone. Each data set consisting of individual test molecules at different concentrations was acquired on a single set of sensors to ensure consistency between measurements. In all tests, fluid was flowed over the crystals at 100 μL/min using an Ismatic IPC High Precision Multichannel Dispenser peristaltic pump (Wertheim, Germany). When received, the QCM-D sensors were treated with oxygen plasma for 10 minutes and then immediately immersed in a 2% SDS solution and allowed to sit for at least 30 minutes. The sensors were rinsed in Milli-Q water and dried under a stream of dry N_2. Immediately before conducting an experiment, the sensors were again treated with oxygen plasma for 10 minutes, placed into the measurement apparatus, and allowed to equilibrate their resonance under 100 μL/min flow of buffer solution.

For QCM-D measurements, SLBs were formed using the VF method.[45] Vesicle stock solutions (5 mg/mL) were diluted to 0.1 mg/mL in buffer and introduced to the sensor chamber. Adsorption of the vesicles to the surface and subsequent fusion were ensured by following the QCM-D traces over time. The formed bilayer was then washed with buffer for ~45 minutes. Biosurfactant solutions were added to the flow chamber and allowed to interact with the bilayer for 45 minutes. The bilayer was then washed with buffer to observe the desorption of biosurfactants from the bilayer over time. Representative QCM-D traces are shown for a single sensor in the results reported below, but further data analysis

described and included in Figure S4 is from three or four (n=3–4) independent experiments run simultaneously on different crystals. During experiments, the measurement chamber was held at 25 ± 0.5 °C. Immediately following each experiment, the sensors were placed in a 2% SDS solution for 30 minutes, washed in Milli-Q water, and then dried under N_2 gas before storage.

Calcein Leakage Assay.

Calcein leakage assays were performed in 96-well microtiter plates. In each well, a 10 μL aliquot of calcein vesicles (at a concentration of 1 mM DOPC by monomer) was combined with 90 μL of a biosurfactant solution. The plate was allowed to sit for 5 minutes and then the fluorescence intensity of the solution was read with an excitation of 480 nm and emission of 525 nm using a Tecan Infinite 200 Pro plate reader. All tests were repeated three times (n=3) for each batch of vesicles and were performed with three (n=3) independently produced batches of vesicles for a total of nine (n=9) fluorescence measurements. Statistical significance against the buffer control was determined using a one-way ANOVA with all nine normalized replicates for each condition used that was corrected for multiple comparisons using Dunnett's method. The fluorescence intensity for each reading was normalized using a procedure adapted from other publications and summarized in Equation 2 where: FI is the fluorescence intensity of the test solution, FI_{Buffer} is the fluorescence intensity of the calcein vesicles in buffer as the negative control, and $FI_{TX\text{-}100}$ was the fluorescence intensity of a vesicle solution containing 1% Triton X-100 (which is known to lyse vesicles) as a positive control.[48]

$$Normalized\ Flourescense = \frac{FI - FI_{Buffer}}{FI_{TX-100} - FI_{Buffer}} \quad \text{(Eq. 2)}$$

Free Energy Calculations.

Molecular dynamics simulations with umbrella sampling[49] were performed to obtain potentials of mean force (PMFs) for the translocation of 3-oxo-C12-AHL, 3-oxo-C12-HS, two rhamnolipids with 10 carbons in the tail with one (rha-C10-C10) or two (rha-rha-C10-C10) rings in the head group, glycerol monolaurate (GML), and lauric acid across a DOPC bilayer containing 128 lipid molecules. All systems were modeled using the CHARMM36 force field with the TIP3P water model.[50] Molecular structures and force field parameters were generated using the CHARMM-GUI Input Generator.[51,52] Verlet lists were generated using a 1.2 nm neighbor list cutoff. Van der Waals interactions were modeled with a Lennard-Jones potential using a 1.2 nm cutoff that was smoothly shifted to zero between 1.0 nm and 1.2 nm. Electrostatic interactions were calculated using the smooth Particle Mesh Ewald method with a short-range cutoff of 1.2 nm, grid spacing of 0.12 nm, and 4^{th} order interpolation. Bonds were constrained using the LINCS algorithm. All systems were energy minimized using the steepest descent method. Simulations were performed in the *NPT* ensemble using a leapfrog integrator with a 2-fs timestep. For equilibration, the temperature was maintained at 310.15 K using a Berendsen thermostat with a time constant of 1.0 ps and the pressure was maintained at 1 bar using a semi-isotropic Berendsen barostat with a time constant of 5.0 ps and a compressibility of 4.5×10^{-5} bar^{-1}. For umbrella sampling,

the temperature was maintained at 310.15 K using a velocity-rescale thermostat with a time constant of 1.0 ps and the pressure was maintained at 1 bar using a semi-isotropic Parrinello-Rahman barostat with a time constant of 5.0 ps and a compressibility of 4.5×10^{-5} bar^{-1}. All simulations were performed using Gromacs 2016.[53]

Umbrella sampling was performed using the *z*-component of the distance between the molecule center of mass and bilayer center of mass (denoted as *z*) as a collective variable. Each umbrella sampling calculation was performed using independent windows separated by 0.1 nm from $z = 0$ nm to $z = 4$ nm with $z = 0$ nm corresponding to the bilayer midplane. At least 41 windows were used for each molecule; 2 additional windows were added for 3-oxo-C12-AHL and rha-C10-C10 and 1 additional window was added for GML. In each case, the number of windows was selected to obtain convergence and ensure that the PMF was symmetric around $z = 0$. Harmonic restraints with force constants ranging from 200 kJ mol^{-1} nm^{-2} to 1500 kJ mol^{-1} nm^{-2} were applied to restrain sampling to a given value of *z*. Each window was equilibrated for 5 ns in the NPT ensemble and then sampled for 32 ns. The last 24 ns of this trajectory were split into two independent 12-ns blocks and used to compute two PMFs as a function of z using the Weighted Histogram Analysis Method.[54] Plots demonstrating PMF convergence are shown in the Supporting Information.

Results and Discussion

To launch our investigations, we performed a series of initial studies to gauge the ability of and extent to which bacterial cultures (or supernatants obtained from bacterial cultures) can alter model lipid membrane systems. *P. aeruginosa* was chosen as a model organism for this study because it is a well-studied opportunistic pathogen, whose lipophilic QS signals and related bio-toxins have been linked to negative outcomes in both environmental and clinical settings.[55–58] We briefly describe the results of these experiments to provide a framework for the discussion of more detailed and systematic studies described below. For these initial experiments, we contacted supported lipid bilayers (SLBs) formed from DOPC with the supernatants of 24-hour cultures of *P. aeruginosa*. We selected SLBs as a model system for these initial studies rather than other lipid membrane systems (such as giant unilamellar vesicles, or GUVs), because they are compatible with a wide range of surface characterization techniques, including acoustic sensors (QCM-D)[59] and fluorescence microscopy,[37,60] and can be prepared using a variety of methods.[45,46,61] DOPC was chosen as a model lipid because it is widely used as a simple laboratory model for mammalian membranes, it is fluid at room temperature,[62] and it has been previously used by other groups to characterize the interactions of analytes with lipid membranes, thereby facilitating comparisons between the results of those past studies and the new experiments with the amphiphiles reported here.[37,63–65] To facilitate visualization by optical microscopy, the lipid membranes were doped with 0.1 wt% of the fluorescently labeled lipid Rho-DPPE. In all of the fluorescence microscopy experiments described here, SLBs were formed on NaOH-treated glass in an Ibidi flow cell using the vesicle fusion (VF) technique, unless otherwise noted (see Methods for additional detail).[45] The adsorption and rupture of lipid vesicles into a SLB was monitored by optical microscopy (Video S1) and the fluidity of the SLBs was confirmed by a qualitative FRAP experiment (Video S2) before the introduction of bacterial supernatants or biosurfactants to the bilayers.

The introduction of cell-free *P. aeruginosa* culture supernatants to SLBs composed of DOPC resulted in large-scale and visually apparent reformations of the bilayers that are shown in the sequence of time lapse fluorescence micrographs included in Figure 2. We observed the growth of long, thin, bright red structures on the surfaces of the bilayers within the first minute of initiating the flow of supernatant into the flow cell. These structures ranged from 1–10 microns to hundreds of microns long (in many cases, longer than the observable field of view; Figure 2B). Some of these structures completely retracted into the underlying bilayer over the course of several minutes to form large pseudo-circular patches of increased fluorescence intensity (Figure 2C). In all of the fluorescence micrographs shown here and in the studies described below, the direction of flow was from the bottom to the top of the field of view, and thus the long, thin structures observed in Figure 2 were aligned in the direction of flow.

The changes in bilayer structure and associated dynamics described above and shown in Figure 2 are similar to the restructuring of SLBs reported in past studies when SLBs were placed in contact with certain natural and synthetic surfactants.[37,60,63–65] In those studies, the presence of long, thin structures and pseudo-circular structures were interpreted to result from the formation of hollow microtubules and thin, water-filled, hemispherical caps. Cartoon representations (both top-down and side view) of these structures are shown in Figure 3. Those past reports provide a framework for probing and interpreting the membrane restructuring observed in our experiments in the presence of bacterial supernatants. While there are many components present in bacterial supernatants that could interact with SLBs, the similarities in the membrane reformations observed in Figure 2 to those previously reported for SLBs in contact with natural and synthetic surfactants suggested the possibility that the membrane restructuring observed in our experiments could be promoted by amphiphilic species present in the supernatant.[37,60,63–65]

In the experiments above, we used culture supernatant collected after 24 hours of *P. aeruginosa* growth, which has been previously shown to contain at least two amphiphilic species: the QS signal 3-oxo-C12-AHL and the QS-regulated biosurfactant rhamnolipid (Figure 1).[66] Rhamnolipid is a well-characterized bio-surfactant and is known to interact with and disrupt mammalian cell membranes.[67,68] The interactions of 3-oxo-C12-AHL with lipid membranes is less well understood, with several recent reports suggesting that it can intercalate into membranes[27,28] and lead to a depolarization of vesicle membranes[30] and the disruption of lipid rafts.[31] However, to the best of our knowledge, the large-scale reformation and remodeling of lipid membranes to form structures such as those shown in Figure 2 has not yet been reported. As noted above, the potential ability of these amphiphiles, either alone or in combination, to promote large-scale membrane remodeling bears on many interesting biological questions (e.g., underlying potential QS mechanisms, signal potency, interspecies signaling, and impacts on host cells) and has the potential to inform the design of new classes of soft materials that can interact with bacterial communities in new ways (e.g., for the development of novel sensors or smart drug delivery vehicles, etc.). These questions and the observations in Figure 2 motivated additional studies of the interactions of 3-oxo-C12-AHL and rhamnolipid with lipid membranes described in the sections below.

Characterization of Interactions of 3-oxo-C12-AHL and 3-oxo-C12-HS with DOPC Membranes Using Fluorescence Microscopy

We began our studies to systematically characterize the interaction of SLBs with components of bacterial supernatants by focusing on the signaling molecule 3-oxo-C12-AHL. Here we note that 3-oxo-C12-AHL has a homoserine lactone head group that can hydrolyze in aqueous media to form 3-oxo-C12-HS (Figure 1).[36] AHL head group hydrolysis occurs relatively rapidly (especially in *P. aeruginosa* cultures that become alkaline over time; $t_{1/2}$= ~10 hr at pH 8)[69,70] and yields an anionic compound that also has an amphiphilic structure and, as a result, has the potential to interact with membranes. It is, thus, important to note that any bacterial supernatant or solution containing 3-oxo-C12-AHL at pH ≥ 7 will likely consist of a mixture of these two components. To set the stage for understanding the interactions of 3-oxo-C12-AHL and 3-oxo-C12-HS, or combinations of these two amphiphiles, with lipid membranes, we measured the surface activity of each compound at the air-water interface using a Wilhelmy plate (Figure S1A; see Methods for details).[47]

Those studies revealed that 3-oxo-C12-AHL is more surface active than 3-oxo-C12-HS, which exhibited lower surface tensions at all concentrations tested (e.g., 46.7 mN/m as compared to 57.3 mN/m at 200 μM, respectively; see Figure S1A for all concentrations tested). Additionally, 3-oxo-C12-AHL exhibited a break in a plot of surface tension vs. concentration (denoted by an arrow in Figure S1), suggesting that it aggregates at a concentration between 100 μM and 125 μM under the conditions used here. The location of this break occurs in a range that is generally consistent with the value reported for the critical aggregation concentration (CAC) for this AHL in our past study, using a combination of light scattering and measurements of surface tension in water (88 ± 20 μM and 97 ± 11 μM, respectively; see that past study for a more detailed discussion on the solution-phase self-assembly of 3-oxo-C12-AHL in aqueous media).[26] In contrast, 3-oxo-C12-HS did not exhibit a break in plots of surface tension vs. concentration in the range of concentrations examined in this study; as a result, we conclude that this hydrolyzed compound does not aggregate in this range of concentrations. These results, taken together, suggest that the chemical hydrolysis of the homoserine lactone head group of 3-oxo-C12-AHL alters its physical behavior in solution and at interfaces, leading to 3-oxo-C12-AHL being more surface active than 3-oxo-C12-HS. We will return to these observations again in the discussion below.

Additional fluorescence microscopy experiments similar to those described above with culture supernatants revealed that 3-oxo-C12-AHL and 3-oxo-C12-HS promote large differences in the structural reformations of DOPC SLBs. Figure 4 shows fluorescence microscopy images of SLBs after exposure to continuous flows of solutions containing different concentrations of 3-oxo-C12-AHL or 3-oxo-C12-HS for periods of 360 sec (additional images of bilayer reformation at intermediate timepoints can be found in Figures S2A and 2B). Images of SLBs that were subjected to the flow of buffer alone for at least 360 sec are shown in Figure 4A,B and reveal that flow alone and exposure to buffer do not cause observable large-scale reformation.

Figure 4C,D shows images of SLBs after the introduction of 3-oxo-C12-AHL (Figure 4C) or 3-oxo-C12-HS (Figure 4D) at 30 μM, which was the lowest concentration tested. This concentration is representative of AHL concentrations measured to be in planktonic cultures of *P. aeruginosa* after 24 hours of growth.[66] Within one minute of introduction of 30 μM 3-oxo-C12-AHL to the flow cell, we observed the formation of tubules ~5–40 μm long on the surface of the bilayer. These tubules were often observed to retract and collapse into hemispherical caps within 5–180 sec of forming. This behavior contrasted to that of SLBs treated with 30 μM 3-oxo-C12-HS solutions, which we observed to form extended tubules (~50 μm in length) that persisted on the surface of the bilayer and did not appear to retract or collapse on the timescale of the experiment. The results shown in Figure 4C,D fall within the range of observations made using bacterial supernatants (in Figure 2), as well as those in past studies using synthetic surfactants,[37,60,64] and suggest that AHLs (and their hydrolyzed derivatives) alone can promote large-scale reformation at biologically relevant concentrations.

To explore this phenomenon further, we conducted additional experiments at concentrations of 3-oxo-C12-HS and 3-oxo-C12-AHL of up to 200 μM, a concentration that is above what is observed in planktonic bacterial cultures, but that is relevant in the context of elevated concentrations of AHL reported to be present in bacterial biofilms.[71] This is also, in our hands, the highest concentration at which 3-oxo-C12-AHL is soluble in the buffers used here. As shown in Figure 4, when 50 μM (Panel F), 100 μM (Panel H), 150 μM (Panel J), or 200 μM (Panel L; Video S6) solutions of the hydrolyzed, 3-oxo-C12-HS compound were introduced to SLBs, we observed the formation of tubules ranging from 5–100 μm in length. These results are consistent with the behaviors observed after the introduction of 30 μM of 3-oxo-C12-HS to SLBs (Figure 4C), but with an increased number of tubules at elevated concentrations. In some cases, we observed a small number of the tubules to retract and form hemispherical caps at these higher concentrations (for example, see Figure 4I). However, the vast majority of tubules did not retract or form hemispherical caps, and tubules were the predominant restructuring phenomenon observed when SLBs were exposed to solutions containing 3-oxo-C12-HS.

The introduction of 3-oxo-C12-AHL to SLBs resulted in bilayer reformation that was more complex than that observed for 3-oxo-C12-HS. At 50 μM (Figure 4E), 3-oxo-C12-AHL promoted membrane restructuring similar to that observed at 30 μM (Figure 4C), where smaller tubules formed within the first minute of the experiment, many of which quickly collapsed into hemispherical caps, and some of which persisted throughout the time of the experiment. At higher concentrations of 100 μM (Figure 4G), 150 μM (Figure 4I), and 200 μM 3-oxo-C12-AHL (Figure 4K; Video S7), combinations of hemispherical caps and extended tubules were also observed. However, in contrast to experiments at lower concentrations of 3-oxo-C12-AHL, we observed many more long, extended tubules that were several hundred microns in length, reminiscent of what we observed in Figure 2 and as described above for experiments using bacterial supernatants, as well as tubule bundles. We note that the critical aggregation concentration (CAC) of 3-oxo-C12-AHL is ~100 μM.[26] The differences in tubule formation observed at these higher concentrations relative to lower concentrations could therefore correlate to the extent of 3-oxo-C12-AHL aggregation, a factor that is known to impact the interaction of amphiphilic species with

lipid membranes.[63,64] In addition to the tubules and hemispherical caps described above, at 150 μM (Figure 4I) and 200 μM (Figure 4K; Video S7) we observed the flow of fluorescent material across the field of view in the direction of flow, suggesting that 3-oxo-C12-AHL at these high concentrations can undergo processes that result in the removal or dissolution of lipid material from the bilayer. We note here that our as-prepared SLBs contain punctate spots of red fluorescence (Figure 4A,B) prior to the introduction of any compounds. These punctate spots are often observed in SLBs formed by the vesicle fusion method and are typically interpreted as surface-bound vesicles that did not rupture during bilayer formation.[72] We also observed the formation of tubules and hemispherical caps in experiments where 200 μM 3-oxo-C12-AHL was introduced SLBs formed using an alternative bicelle fusion method that does not involve the use of vesicles (see Methods and Video S8),[46] suggesting that the changes in morphology observed above do not arise from artifacts associated with the presence of unruptured vesicles.

Additional experiments revealed that the formation of these surface features was, in many cases, at least partially reversible upon the removal of compound and washing with buffer. Figure S3 shows images of a bilayer analogous to the one shown in Figure 4 after rinsing with buffer for at least eight minutes. These images show that tubules can retract and collapse into hemispherical caps, and that caps can subsequently shrink in size and, in some cases, disappear from the surface of the bilayer for all concentrations of 3-oxo-C12-HS and 3-oxo-C12-AHL tested. At higher concentrations of 3-oxo-C12-AHL (150 μM and 200 μM (Figure S3; insets in panels (H,J)), we also observed circular areas of decreased fluorescence, suggesting that some local removal of bilayer material could occur under these conditions. The observation of these darker patches is consistent with our observations, as discussed above, of fluorescent material floating across the field of view when high concentrations of 3-oxo-C12-AHL were introduced to the bilayers.

Taken together, these results are consistent with the results of our initial experiments performed with bacterial supernatant and show unambiguously that AHLs can cause large-scale membrane reformations. Additionally, our results show that 3-oxo-C12-AHL head group hydrolysis can change the physical properties of AHL and lead to differences in membrane reformation. The results described thus far provide additional evidence for conclusions emerging from a growing body of work suggesting that 3-oxo-C12-AHL can interact with lipid bilayers in ways that lead to changes in physical properties and structure.[27,28,30,31] To our knowledge, the results reported here are the first to demonstrate that the QS signal 3-oxo-C12-AHL and its hydrolysis product 3-oxo-C12-HS can interact with SLBs in ways that lead to large-scale structural reformation in the bilayer. Additional experiments to explore differences in the interactions of 3-oxo-C12-AHL and 3-oxo-C12-HS with lipid membranes, and the implications of these differences in behavior, are described in the sections below.

Characterization of the Interactions of 3-oxo-C12-AHL and 3-oxo-C12-HS with DOPC Membranes Using QCM-D

The results described above demonstrate that large-scale membrane remodeling occurs when a QS signal of an important bacterial pathogen, 3-oxo-C12-AHL, interacts with a model

lipid membrane. Those results also reveal qualitative differences between the behaviors mediated by 3-oxo-C12-AHL and its naturally occurring hydrolysis product 3-oxo-C12-HS. To provide additional quantitative insight into these processes, we used quartz crystal microbalance with dissipation (QCM-D) to measure differences in the response of DOPC SLBs when introduced to solutions of 3-oxo-C12-AHL or 3-oxo-C12-HS (see Methods for additional details). After the SLBs were formed on SiO_2-functionalized quartz crystals using the vesicle fusion method[45] and washed with buffer, they were exposed to a flow of 3-oxo-C12-AHL or 3-oxo-C12-HS solutions (100 μL/min) at various concentrations. Figure 5 shows the changes in frequency (Δf, blue lines) and dissipation (ΔD, orange lines) in SLBs upon exposure to 3-oxo-C12-AHL (solid lines) or 3-oxo-C12-HS (dashed lines) at various concentrations and after a subsequent buffer wash (Δf and ΔD values at t=0 min correspond to values for a stable SLB assembled on the quartz crystal prior to the experiment). The solid arrows in Figure 5 indicate the time at which solutions containing compound were added to SLBs, while the dashed arrows indicate the time at which buffer washes were initiated. All data shown are representative QCM-D data sets of either three or four replicates. Full data analysis of all trials (mean and standard deviation of each concentration for each compound) can be found in Figure S4 and provide the Δf and ΔD values referred in the text below.

In general, we observed the introduction of 3-oxo-C12-AHL to (i) lead to more dramatic restructuring in DOPC SLBs, as indicated by the larger positive change in ΔD, and (ii) adsorb in greater amounts to the bilayer, as suggested by larger negative changes in Δf, when compared to 3-oxo-C12-HS at a given concentration (Figure 5 and summarized in Figure S4). When 3-oxo-C12-AHL was introduced to the bilayer at 50 μM (Figure 5A), 75 μM (Figure 5B), and 100 μM (Figure 5C), we observed similar changes in frequency (-2.5 ± 0.1 Hz, -2.9 ± 0.3 Hz, and -4.0 ± 0.3 Hz) and dissipation ($1.2 \pm 0.2 \times 10^{-6}$, $1.5 \pm 0.2 \times 10^{-6}$, and $1.1 \pm 0.1 \times 10^{-6}$). At the higher concentrations of 125 μM (Figure 5D), 150 μM (Figure 5E), and 200 μM (Figure 5F), which are above the CAC measured for 3-oxo-C12-AHL, we generally measured larger changes in Δf and ΔD at increasing concentrations, recording shifts of (-6.5 ± 0.5 Hz and $2.8 \pm 0.4 \times 10^{-6}$), ($-6.3 \pm 2.2$ Hz and $3.1 \pm 0.7 \times 10^{-6}$), and ($-8.8 \pm 1.5$ Hz and $4.0 \pm 0.5 \times 10^{-6}$), respectively. This apparent change in the general response in the bilayer below and above the CAC of 3-oxo-C12-AHL is similar to that observed qualitatively in our fluorescence microscopy results (Figure 4). Additionally, the larger changes in frequency suggest that there is a greater mass of 3-oxo-C12-AHL adsorbing to the bilayer at higher concentrations. Upon washing the bilayers with buffer, all SLBs treated with 3-oxo-C12-AHL exhibited positive changes in Δf and negative changes in ΔD, suggesting that bilayer reformation is semi-reversible, in agreement with behaviors observed by fluorescence microscopy above. Together, these results further suggest that 3-oxo-C12-AHL is interacting with lipid bilayers in ways that lead to membrane restructuring in a semi-reversible fashion under all conditions examined here.

In contrast to 3-oxo-C12-AHL, the introduction of 3-oxo-C12-HS led to smaller shifts in Δf and ΔD in the SLBs. As shown in Figure 5 and summarized in Figure S4 the introduction of this hydrolyzed compound at 50 μM (Figure 5A) led to shifts of -0.9 ± 0.3 Hz and $0.3 \pm 0.1 \times 10^{-6}$ for Δf and ΔD, respectively. These smaller changes in both Δf and ΔD were also observed for 3-oxo-C12-HS at the higher concentrations of 100 μM (Figure 5C), 150 μM (Figure 5E), and 200 μM (Figure 5F) with shifts of (-1.0 ± 0.6 Hz and $0.6 \pm 0.2 \times 10^{-6}$),

(0.0 ± 0.4 Hz and 0.7 ± 0.1 $\times 10^{-6}$), and (−0.4 ± 0.8 Hz and 0.8 ± 0.1 $\times 10^{-6}$) for Δf and ΔD, respectively. Similar to 3-oxo-C12-AHL, washing these treated bilayers with buffer also led to partial recovery of Δf and ΔD values, suggesting a semi-reversible desorption of 3-oxo-C12-HS from the membranes.

Taken together, the results above suggest that 3-oxo-C12-HS interacts with SLBs in a manner that leads to lower mass adsorption and membrane remodeling that is less extensive (or at least very different) than those observed for 3-oxo-C12-AHL at similar concentrations. The observation of lower mass adsorption for 3-oxo-C12-HS is consistent with our surface tension measurements, which, as discussed above, reveal that the hydrolyzed compound has lower surface activity than 3-oxo-C12-AHL at air-water interfaces. These QCM-D results are also consistent with the observation and dynamics associated with the formation of microtubules and hemispherical caps observed in our fluorescence microscopy studies, which again are in line with previous reports documenting the interaction of 3-oxo-C12-AHL with lipid membranes and associated changes in bilayer properties.[27,28,30,31] These results do not provide mechanistic insight into what may be occurring, at a molecular level, to lead to these large changes in morphology. We return in sections below to the results of molecular dynamics (MD) simulations that provide additional perspective on physicochemical differences between 3-oxo-C12-AHL and 3-oxo-C12-HS that are likely to underlie the large changes in behavior observed experimentally here.

Characterization of Interactions of Rhamnolipid with DOPC Membranes

As introduced above, *P. aeruginosa* and several related species use 3-oxo-C12-AHL for QS to regulate many group behaviors, including the production of virulence factors such as rhamnolipid,[23] a biosurfactant known to interact with and disrupt lipid membranes.[67,68] Depending on the conditions, 3-oxo-C12-AHL and 3-oxo-C12-HS may therefore exist either alone (e.g., at low population densities; prior to quorum) or in combination with rhamnolipid (e.g., at high population densities; at or above quorum, as was the case in the experiments presented in Figure 2).[66] In view of the latter condition, we also sought to characterize the interaction of rhamnolipid with DOPC SLBs and determine the extent to which it may contribute to membrane remodeling, including the formation of tubules or hemispherical caps, under conditions similar to those examined above for 3-oxo-C12-AHL and 3-oxo-C12-HS. For these experiments, we selected a concentration of 40 μg/mL, which is the concentration of rhamnolipid measured to be present in 24-hour (high population density, or “quorate”) cultures of *P. aeruginosa*.[66]

Figure 6 shows a representative QCM-D trace (Figure 6A) and selected fluorescence microscopy images of DOPC SLBs exposed to a constant flow of rhamnolipid solution (Figure 6B–D) and a subsequent buffer wash (Figure 6E). Within the first minute of introducing rhamnolipid solution to the bilayer, we observed the formation of extended tubule structures, a small proportion of which collapsed into hemispherical caps over the subsequent six minutes of the experiment (Figure 6B–D). As the rhamnolipid solution was flowed across the surface of the bilayer, we observed some fluorescently labeled material and detached tubules moving across the field of view in the direction of flow, suggesting that rhamnolipid was also removing material from the bilayers, as was observed in analogous

studies above for high concentration solutions of 3-oxo-C12-AHL. Characterization by QCM-D revealed positive changes in frequency (Δf) upon exposure of the SLB to rhamnolipid (3.3 ± 0 Hz) and after a subsequent wash of the bilayer with buffer (2.5 ± 0.2 Hz), with smaller changes in dissipation (ΔD) than those observed for 3-oxo-C12-AHL. The positive changes in frequency, consistent with a removal of mass from the bilayer, are consistent with the observation of the loss or removal of fluorescent material from the bilayer by fluorescence microscopy. Experiments using higher concentrations of rhamnolipid (e.g., 100 μg/mL and 200 μg/mL) led to the formation of tubules, but also to more extensive removal of material from the bilayer during exposure and the formation of patches that appeared darker by fluorescence microscopy (Figure S5 Panels D–E and I–J). This observation is consistent with the well-known surfactant properties of rhamnolipid and its ability to disrupt membranes, which is an important part of its biological function as a bacterial virulence factor.[67,68] However, as a result of this behavior, we were unable to draw meaningful quantitative conclusions from the results of our QCM-D experiments at these higher concentrations. We can conclude, however, that rhamnolipid is able to interact with lipid bilayers in ways that lead to similar morphological changes as those observed for AHLs (e.g., both promote reformation into tubules and a small number of caps). It is likely that AHL-induced reformations would occur simultaneously with those promoted by rhamnolipid, with more substantial disruption resulting from the strong surfactant behavior of rhamnolipid. (It is also possible that AHLs and rhamnolipid could act in concert or synergistically when both are present, but that possibility was not investigated or considered further here).

Bilayer Reformation in Unilamellar Vesicles: GUVs and Calcein Leakage

The SLBs used in the experiments above are a useful model and facilitate the characterization of interactions of surfactants with lipid bilayers using QCM-D and fluorescence microscopy on planar surfaces. We note, however, that SLBs are confined systems that are in close proximity to an underlying solid support. The membranes of biological systems and many other types of synthetic materials are, by contrast, free standing and can, therefore, exhibit behaviors that differ from those of SLBs. To confirm general observations made above using SLBs and provide additional insight into the interactions of 3-oxo-C12-AHL, 3-oxo-C12-HS, and rhamnolipid with unsupported lipid membranes, we also conducted experiments with giant unilamellar vesicles (GUVs) composed of DOPC (see Methods for additional details related to fabrication and characterization).[44] Figure 7 shows representative images of a GUV suspended in buffer alone (7A) and in contact with 100 μM 3-oxo-C12-AHL (7B) or 25 μg/mL rhamnolipid (7C). We observed that when either 3-oxo-C12-AHL or rhamnolipid was introduced to the GUVs, the vesicles formed long tubular structures protruding from the outer leaflet of the bilayer (as denoted by the arrowheads in panel 7B). It was more difficult to characterize these tubules because of the dynamic nature of this vesicle system, but these tubules were, in general, similar to those observed in our SLB experiments. Additionally, we note that we did not observe the formation of hemispherical caps in these GUV experiments, likely because free-standing (unsupported) vesicular systems such as GUVs have different mechanisms, relative to SLBs, by which they can relieve asymmetrical bilayer stresses and the formation of hemispherical caps should not occur (and would, otherwise, be difficult to characterize) in these systems.[73]

Overall, approximately 80% of the vesicles in contact with 3-oxo-C12-AHL formed tubules, as opposed to 100% in the rhamnolipid solution and approximately 5% in the buffer control (Figure 7D). These results provide insight into the interaction of these amphiphiles with unsupported lipid membranes that are a better approximation of a cell membrane (or a drug delivery vehicle, etc.) and suggest that the results observed in our SLB experiments are not artifacts arising from the surface supported nature of those bilayers or from defects that could be present in those systems.

We performed additional experiments with lipid vesicles to determine if the interactions with 3-oxo-C12-AHL and 3-oxo-C12-HS, and subsequent restructuring to form microtubules, could compromise membrane integrity in ways that could allow for leakage of vesicle contents or promote molecular transport across these membranes. To investigate this further, we used large unilamellar vesicles (LUVs) made of DOPC and loaded with the self-quenching fluorophore calcein, and a previously established calcein leakage assay (see Methods).[43,67] As a control experiment, we first characterized the interaction of rhamnolipid, which is well known to disrupt and dissolve lipid vesicles, with calcein-loaded LUVs.[67] Upon addition of rhamnolipid-containing solution to LUVs, we observed an increase in the fluorescence of the solution at increasing rhamnolipid concentrations (Figure 8A), which is consistent with vesicle disruption and the release of encapsulated calcein. This is consistent with past studies and the well-known biosurfactant properties of rhamnolipid.[67]

As shown in Figure 8B, both 3-oxo-C12-AHL and 3-oxo-C12-HS also led to low but statistically significant levels of calcein leakage from DOPC vesicles at concentrations above 68 μM. 3-oxo-C12-AHL exhibited an approximately linear increase in the fluorescence signal with increasing concentration up to ~180 μM, the highest concentration tested here. In contrast, 3-oxo-C12-HS resulted in low levels (approximately 1.5% leakage) of calcein fluorescence at all concentrations above ~25 μM, a level that is statistically significant from the buffer controls. The difference in the extent of leakage shown in Figure 8 is consistent with the differences in bilayer reformation promoted in 3-oxo-C12-AHL and 3-oxo-C12-HS observed by fluorescence microscopy and QCM-D in SLBs. These compounds have different head groups, one of which is charged and one of which is neutral, which could lead to differences in their propensity to adsorb to, intercalate into or translocate across lipid membranes, and thus lead to differential changes in membrane structure or integrity.[16] This result is, to our knowledge, the first observation of the leakage of contents across a lipid membrane promoted by an AHL-type bacterial QS signal and could, with further study, provide insight into the previously unexplored biological roles of these compounds (e.g., as an independent virulence factor that is potentially capable of compromising host-cell membranes), or the ways in which they might interact with or trigger responses in synthetic lipid membranes (e.g., in the context of drug delivery or sensing, etc.). In the section below, we describe the results of MD simulations that provide additional mechanistic insight into factors that govern the behaviors of these molecules at the surfaces of lipid membranes.

Molecular Dynamics Simulations of Amphiphile-Membrane Interactions

The studies above demonstrate that 3-oxo-C12-AHL and 3-oxo-C12-HS behave differently when in contact with lipid membranes. These differences are similar to those observed in

past studies on the interactions of neutral and anionic surfactants in contact with SLBs.[37,60] For example, Cho and coworkers reported that the non-ionic surfactant glycerol monolaurate (GML) led to the formation of tubules that quickly collapsed into hemispherical caps when placed in contact with DOPC SLBs, and that the structurally similar anionic surfactant lauric acid (LA) led largely to the formation of tubules (that did not retract into hemispherical caps; structures of GML and LA shown in Figure S6).[37] In that study, the authors proposed that observed differences in bilayer reformation could arise from differences in the ability of GML and LA to translocate from the outer leaflet of a bilayer to the inner leaflet (e.g. by "flip-flop", or some similar mechanism) after adsorption, thus leading to asymmetric stresses that result in the formation of tubules or caps on the surface of the bilayer. To explore this proposal in further detail and provide insight into the thermodynamic barriers associated with the translocation of 3-oxo-C12-AHL and 3-oxo-C12-HS (and also GML and LA) across DOPC membranes, we performed a series of atomistic molecular dynamics (MD) simulations.

We first calculated the free energy profile for translocating 3-oxo-C12-AHL along the bilayer normal (*z*-direction) of a planar DOPC membrane using umbrella sampling, as shown in Figure 9A, and compared it to the free energy profile of 3-oxo-C12-HS. Snapshots from representative distances along the DOPC bilayer normal (*z*) are shown in Figure 9B. From these free energy profiles, we defined two free energy differences, the partition free energy (ΔG_{par}) and the translocation free energy (ΔG_{trans}), to compare the likelihood of each compound to intercalate into and translocate across the bilayer, respectively (Figure 9C).[74] ΔG_{par} is defined as the difference in free energy between the PMF minimum and the reference state in solution (e.g., $z \geq -4$ nm). ΔG_{trans} is defined as the difference in free energy between the PMF maximum at the bilayer center and the PMF minimum.[74] In these contexts, a more negative value of ΔG_{par} indicates that it is favorable for a compound to partition into the lipid monolayer, and a more positive value of ΔG_{trans} indicates that it is less favorable for a surfactant to translocate across the lipid bilayer. ΔG_{par} (dashed arrows) and ΔG_{trans} (solid arrows) are visually defined in Figure 9A for 3-oxo-C12-AHL and 3-oxo-C12-HS.

As shown in Figure 9A and summarized in Figure 9C, our simulations predict that 3-oxo-C12-HS has a higher ΔG_{trans} than 3-oxo-C12-AHL (ΔG_{trans} = 67.59 kJ/mol and 35.57 kJ/mol, respectively) indicating that it is more difficult for the hydrolyzed 3-oxo-C12-HS to translocate across the lipid bilayer than it is for 3-oxo-C12-AHL. Our simulations also reveal that 3-oxo-C12-AHL has a more negative ΔG_{par} than 3-oxo-C12-HS, which indicates that 3-oxo-C12-AHL can partition itself into the bilayer more readily than the hydrolyzed compound, as expected in view of its non-ionic head group. This result is consistent with our surface tension and QCM-D measurements above, from which we found 3-oxo-C12-AHL to be more surface active and to a have more mass association with the bilayer than 3-oxo-C12-HS at a given concentration.

In addition to simulations of 3-oxo-C12-AHL and 3-oxo-C12-HS, we performed MD simulations of two representative 10-carbon tail rhamnolipids with one or two rhamnose sugars in the head group (Figures 9C and S7; rhamnolipid is relatively heterogeneous in nature, with the head group number (one or two) and lipid tail length varying with different

bacterial growth conditions).[75] These simulations revealed that having two rhamnose units in the head group leads to a much more negative ΔG_{par} (−31.99 kJ/mol vs. −16.55 kJ/mol) and, therefore, is predicted to promote more favorable partitioning into the bilayer than rhamnolipid with a single sugar head group. However, the number of head group rhamnose units did not impact ΔG_{trans} significantly (62.68 kJ/mol vs. 56.90 kJ/mol). Finally, to permit comparisons and provide further insight into the interactions of LA and GML with DOPC SLBs, we calculated their PMFs along the bilayer normal, which revealed that nonionic GML has values of ΔG_{par} and ΔG_{trans} that are both lower than anionic LA (Figure 9C; Figure S7). These results suggest that GML should be more likely to interact with and translocate across the membrane, as previously predicted by Cho and coworkers.[37]

The relative magnitudes of ΔG_{par} and ΔG_{trans} calculated for the four single-tailed amphiphiles described above reveal the nonionic compounds 3-oxo-C12-AHL and GML to be more likely to intercalate into and translocate across DOPC membranes than the anionic compounds 3-oxo-C12-HS and LA. These differences in the propensity of a given amphiphile to partition itself into the bilayer correlate to the magnitude of response measured in the QCM-D experiments with 3-oxo-C12-AHL and 3-oxo-C12-HS in this study and with GML and LA in past studies.[37] Although it is not possible to explicitly compare the experimental QCM-D responses from these two different studies, we note that the relative magnitudes of the QCM-D response for these four compounds (GML > 3-oxo-C12-AHL > LA > 3-oxo-C12-HS) are generally in line with the predictions of our MD simulations (Figure 9C, Figure 5 and past work by Cho and coworkers[37]). Because ΔG_{par} describes an equilibrium between membrane-bound and solution-phase species, a more negative ΔG_{par} would suggest that a higher proportion of the molecules would associate with a bilayer at a given concentration. This higher degree of association would be subsequently reflected as a larger Δf, as more mass is associated to the surface of the bilayer, and lead to increased membrane restructuring, as measured by ΔD, due to increased lateral stresses in the bilayer, as discussed below.

Discussion of Potential Mechanisms for Bilayer Reformation

The combined results of our experimental and MD simulation studies provide support for the view that the differences in the restructuring of lipid bilayers observed here and in past studies[37] are driven by the differences in the ability of 3-oxo-C12-AHL and 3-oxo-C12-HS (or GML and LA) to translocate across the bilayer. The non-ionic amphiphiles 3-oxo-C12-AHL and GML, which predominantly lead to the formation of hemispherical caps in fluorescence microscopy experiments, have lower predicted barriers to translocation than the anionic compounds 3-oxo-C12-HS and LA, which lead to the formation of predominantly extended tubule structures. Overall, these results are consistent with a physical picture in which bilayer remodeling is driven by changes or differences in asymmetric stresses that develop between the outer and inner leaflets of a bilayer upon intercalation and/or translocation of an amphiphile.[7,16]

When an amphiphile inserts into the outer leaflet of a bilayer, it imparts an asymmetric, lateral stress on that leaflet that is not immediately matched by the inner leaflet. If the area of a bilayer is fixed, as would be the case in our SLB experiments or in a vesicle of fixed

volume, a molecule that has a high barrier to translocation (or “flip-flop”), would continue to accumulate in the outer leaflet and continue to increase asymmetrical stress, driving the formation of regions of high curvature (such as tubules).[7] For amphiphiles with low translocation barriers, asymmetrical stress would be expected to be relieved rapidly by flip-flop, leading to the formation of lower curvature structures (such as hemispherical caps) as a means of relieving symmetric bilayer stresses.[7] For amphiphiles with intermediate barriers to translocation, this framework would predict the initial formation of high-curvature tubules that would, over time, transition to lower curvature structures such as hemispherical caps as translocation across the bilayer occurs and initial asymmetric stresses are relieved.[7,16] In line with these predictions, amphiphiles with high predicted barriers to translation (3-oxo-C12-HS, rhamnolipid, and LA) generally lead to the formation of tubules that persist over the time course of fluorescence microscopy experiments, and amphiphiles with lower barriers to translocation (3-oxo-C12-AHL and GML) are observed to initially form tubules that transition to become hemispherical caps, suggesting that these two nonionic amphiphiles are able to translocate to inner leaflets on the timescales of these experiments.

The results above do not rule out other contributions to the reformation of these bilayers, including potential impacts that head group structure could have on spontaneous curvature and the formation of surfactant rich domains that could also lead to the formation of tubules and hemispherical caps.[76] However, the experiments in which we observed reversibility of amphiphile-induced reformation upon washing with buffer (see Figure S4 and discussion above) provide further support to the proposal that asymmetrical stresses between bilayer leaflets lead to the observed differences in bilayer reformation (Figure S3; past work by Cho and coworkers[37]). Here we assume that washing the bilayer with buffer and removing amphiphiles from solution can lead to an environment in which desorption of amphiphile from the outer leaflet of a bilayer can occur readily. In the case where an amphiphile is slow to translocate to the inner leaflet (e.g., 3-oxo-C12-HS, rhamnolipid, and LA), as the bilayer is washed and the amphiphile desorbs from the bilayer into solution, it subsequently relieves the asymmetrical stress present in the outer leaflet, promoting a transition from high curvature structures (e.g., tubules) to low curvature structures (e.g., hemispherical caps) and ultimately, in the limit of complete amphiphile desorption, to a flat bilayer. The shrinking and disappearance of tubules and caps was observed experimentally when SLBs that had been introduced to 3-oxo-C12-HS, rhamnolipid, and LA, were subsequently washed with buffer (Figure S3; see also past work by Cho and coworkers[37]). Alternatively, for amphiphiles with low thermodynamic barriers to translocation (e.g., 3-oxo-C12-AHL and GML) that can flip-flop readily, amphiphiles in the inner leaflet can translocate back to the outer leaflet (e.g., as desorption from the outer leaflet occurs) to equilibrate stresses in the bilayer and eventually themselves desorb from the bilayer leading, ultimately, to a flat bilayer. In our experiments, we frequently observed the shrinking and, in some cases, the disappearance of hemispherical caps in bilayers that had been treated with 3-oxo-C12-AHL (and similar behavior was previously reported for GML[37]) upon washing with buffer.

Overall, the trends in amphiphile induced reformation observed experimentally here are strongly correlated to the thermodynamic barrier of the interacting amphiphile to translocation across the membrane and, thus, can be described by differences in asymmetric stresses that are likely to be present in the bilayers. In addition to providing insight

into fundamental interactions of these natural nonionic and anionic amphiphiles with lipid membranes, our results also hint at experimental frameworks that could be used to characterize the timescales on which amphiphiles may translocate (e.g., by characterizing processes associated with the dynamics involved in the formation and deformation of tubules and hemispherical caps). Finally, the differences in membrane response characterized here could potentially be tuned or exploited to design self-assembled systems that respond selectively, and with a desired mode of membrane restructuring, to these or other specific classes of bacterial amphiphiles, providing new avenues for the design of sensing platforms with more selective responses or drug delivery vehicles that respond specifically to communities of bacteria that produce that amphiphile.

Characterization of Bilayer Remodeling Mediated by Mixtures of Amphiphiles Produced by Communities of Bacteria

We return now to a discussion of the results shown in Figure 2, which demonstrate that supernatants obtained from 24-hour cultures of *P. aeruginosa* can promote large-scale reformations in SLBs. The results above show that 3-oxo-C12-AHL, 3-oxo-C12-HS and rhamnolipid can each, individually, interact with lipid membranes and promote large-scale reformation. At 24 hours, cultures of *P. aeruginosa* should contain all three of these amphiphiles. We conducted additional experiments using SLBs and cell-free supernatants obtained from 6-hour cultures of *P. aeruginosa* that have been measured to contain approximately 10 μM 3-oxo-C12-AHL (and thus likely some low concentration of 3-oxo-C12-HS) and either no or low (< 5 μg/mL) concentrations of rhamnolipid.[66] As shown in Figure 10(A–C), these supernatants did not result in large-scale reformations similar to those observed the studies above by fluorescence microscopy. We did occasionally observe the formation of hemispherical caps (e.g., Figure 10C), but these features were relatively rare under the conditions and with the methods used here.

We note that the ~10 μM concentration of 3-oxo-C12-AHL in these supernatants is substantially lower than the concentrations of 3-oxo-C12-AHL used in the systematic studies above (Figure 4; 30 μM). We therefore conducted additional experiments using 24-hour supernatants of a mutant strain of *P. aeruginosa* (ΔrhlA) that is unable to produce rhamnolipid or its amphiphilic precursors under any conditions, even at high population densities, yet still produces 3-oxo-C12-AHL at native levels.[40,77] The results of that experiment are shown in Figure 10(D–F) and reveal the formation of tubules on the surface of the bilayer, a small proportion of which collapsed into hemispherical caps. This result likely arises from higher concentrations of 3-oxo-C12-AHL and its hydrolysis product 3-oxo-C12-HS in solution after 24 hours of bacterial growth. We consider it likely that 3-oxo-C12-AHL and 3-oxo-C12-HS could act in concert to promote bilayer remodeling. Further support for this is provided by experiments demonstrating that defined mixtures of these two amphiphiles can lead to membrane reformations in SLBs (see Figure S9; these results at least suggest that combinations of 3-oxo-C12-AHL and 3-oxo-C12-HS do not prevent bilayer reformation). In any case, the results of experiments with this mutant bacterial strain demonstrate that the production of 3-oxo-C12-AHL by bacteria can promote membrane remodeling in the absence of rhamnolipid. In a broader context, we note that 3-oxo-C12-HS is generally considered to be biologically inactive as a mediator of QS.[78]

Our results reported above (Figures 4, 5, 8) suggest that this hydrolyzed product, which can accumulate in bacterial cultures over time, could play other important roles in communities of bacteria.

The prospect that 3-oxo-C12-AHL and/or 3-oxo-C12-HS alone could promote membrane remodeling leads to intriguing questions and hypotheses about ways in which communities of bacteria may interact with each other, or with other species of bacteria at either low or high population densities. These results could also shed light on ways in which bacteria and communities of bacteria interact with host cells and provide potential guidance for the design and understanding of interactions of bacterial communities with synthetic materials (e.g., lipid-based materials for sensing and responsive drug delivery). Finally, we note that not all bacteria that produce 3-oxo-C12-AHL as their QS signal also produce biosurfactants such as rhamnolipid.[67,77] Our results therefore may also provide insight on how these bacterial species interact with their environment in the absence of biosurfactants or virulence factors that can otherwise interact with and disrupt lipid membranes.

Conclusion

The work reported here demonstrates that the bacterial QS signaling molecule 3-oxo-C12-AHL and its hydrolysis product 3-oxo-C12-HS can interact with model lipid membranes and promote large-scale membrane remodeling, including the formation of tubules and/or hemispherical caps. Our results obtained using fluorescence microscopy and QCM-D demonstrate that these processes are dynamic and reversible, and that they occur both in SLBs and unsupported lipid membranes (e.g., vesicles). Rhamnolipid, a virulence factor produced by *P. aeruginosa* under the control of QS, also promotes similar bilayer reformation but also leads to more substantial disruption and dissolution of bilayers, consistent with the well characterized biosurfactancy of this amphiphile. Additional experiments using a vesicle-based dye leakage assay demonstrated that 3-oxo-C12-AHL and 3-oxo-C12-HS can also facilitate molecular transport across bilayers. MD simulations predict differences in the thermodynamic barriers to translocation of these amphiphiles across the bilayer in ways that are reflected in differences in type and extent of reformation and associated dynamics that are observed experimentally. These differences can be interpreted in terms of an accumulation and relief of asymmetric stresses in the inner and outer leaflets of a bilayer upon the intercalation and translocation of an amphiphile in ways that are similar to past experiments using other natural and synthetic amphiphiles. Finally, our results demonstrate that cultures of bacteria that produce 3-oxo-C12-AHL can promote membrane remodeling in SLBs in the absence of other biosurfactants such as rhamnolipid. Overall, our results suggest potential roles for 3-oxo-C12-AHL and its hydrolysis product that move beyond the context of assessing “self” population density to potential mechanisms for interspecies interactions and control of host cell response. More broadly, the results of these studies with model lipid membranes provide guidance that could be helpful for understanding the range of interactions between bacterial communities and synthetic self-assembled materials (e.g., SLBs and lipid vesicles) commonly used to design environmental sensors and drug delivery vehicles, and in other fundamental and applied contexts. Studies investigating the interactions of structurally diverse, naturally occurring AHLs with model SLBs of increasing complexity are currently underway and will be reported in due course.

Supplementary Material

Refer to Web version on PubMed Central for supplementary material.

Acknowledgements.

Financial support for this work was provided by the NSF through a grant provided to the UW-Madison Materials Research Science and Engineering Center (MRSEC; DMR-1720415). S. J. P. and R. C. V. acknowledge support from the NSF (MCB-1817292). H. E. B. and D. E. M. acknowledge support from the NIH (R35 GM131817). C. G. G. was supported in part by a NSF Graduate Research Fellowship. L. M. C. was supported in part by the UW-Madison NIH Chemistry-Biology Interface Training Program (T32 GM008505). The authors acknowledge the use of instrumentation supported by the NSF through the UW MRSEC (DMR-1720415) and the Extreme Science and Engineering Discovery Environment (XSEDE; ACI-1548562). NMR characterization was performed in facilities in the Department of Chemistry at UW-Madison that are supported by the NSF (CHE-0342998). The authors gratefully acknowledge Prof. Nicholas Abbott (Cornell) and Prof. Joel Pedersen (UW-Madison) for many helpful discussions. We thank Dr. Timothy Smith and Dr. Isabel Foreman-Ortiz for assistance with QCM-D training and for valuable discussions, Christopher Eom and Dr. M. R. Lee for assistance with NMR quantification experiments, and Thomas Polaske for assistance with bacterial cell culture.

References

1. Mura S; Nicolas J; Couvreur P. Stimuli-Responsive Nanocarriers for Drug Delivery. Nat. Mater2013, 12, 991–1003. [PubMed: 24150417]
2. Paliwal SR; Paliwal R; Vyas SPA Review of Mechanistic Insight and Application of pH-Sensitive Liposomes in Drug Delivery. Drug Delivery2015, 22, 231–242. [PubMed: 24524308]
3. Carrion FJ; Delamaza A; Parra JLThe Influence of Ionic-Strength and Lipid Bilayer Charge on the Stability of Liposomes. J. Colloid Interface Sci1994, 164, 78–87.
4. Garcia-Manyes S; Oncins G; Sanz F. Effect of pH and Ionic Strength on Phospholipid Nanomechanics and on Deposition Process onto Hydrophilic Surfaces Measured by AFM. Electrochim. Acta2006, 51, 5029–5036.
5. Cullis PR; de Kruijff B. Lipid Polymorphism and the Functional Roles of Lipids in Biological Membranes. Biochim. Biophys. Acta1979, 559, 399–420. [PubMed: 391283]
6. Frolov VA; Shnyrova AV; Zimmerberg J. Lipid Polymorphisms and Membrane Shape. Cold Spring Harbor Perspect. Biol2011, 3, a004747.
7. Staykova M; Arroyo M; Rahimi M; Stone HAConfined Bilayers Passively Regulate Shape and Stress. Phys. Rev. Lett2013, 110, 028101.
8. Koynova R; Caffrey M. Phases and Phase Transitions of the Phosphatidylcholines. Biochim. Biophys. Acta, Rev. Biomembr1998, 1376, 91–145.
9. Gozen I; Dommersnes P. Pore Dynamics in Lipid Membranes. Eur. Phys. J.: Spec. Top2014, 223, 1813–1829.
10. Shinoda W. Permeability Across Lipid Membranes. Biochim. Biophys. Acta2016, 1858, 2254–2265. [PubMed: 27085977]
11. Torchilin VPRecent Advances with Liposomes as Pharmaceutical Carriers. Nat. Rev. Drug Discovery2005, 4, 145–160. [PubMed: 15688077]
12. Peer D; Karp JM; Hong S; FaroKhzad OC; Margalit R; Langer R. Nanocarriers as an Emerging Platform for Cancer Therapy. Nat. Nanotechnol2007, 2, 751–760. [PubMed: 18654426]
13. Liu QT; Boyd BJLiposomes in Biosensors. Analyst2013, 138, 391–409. [PubMed: 23072757]
14. Tang CY; Zhao Y; Wang R; Helix-Nielsen C; Fane AGDesalination by Biomimetic Aquaporin Membranes: Review of Status and Prospects. Desalination2013, 308, 34–40.
15. Jones MNSurfactant Interactions with Biomembranes and Proteins. Chem. Soc. Rev1992, 21, 127–136.
16. Heerklotz H. Interactions of Surfactants with Lipid Membranes. Q. Rev. Biophys2008, 41, 205–264. [PubMed: 19079805]
17. Miller MB; Bassler BLQuorum Sensing in Bacteria. Annu. Rev. Microbiol2001, 55, 165–199. [PubMed: 11544353]

18. Waters CM; Bassler BLQuorum Sensing: Cell-to-Cell Communication in Bacteria. Annu. Rev. Cell Dev. Biol2005, 21, 319–346. [PubMed: 16212498]
19. Welch M; Mikkelsen H; Swatton JE; Smith D; Thomas GL; Glansdorp FG; Spring DRCell-Cell Communication in Gram-Negative Bacteria. Mol. Biosyst2005, 1, 196–202. [PubMed: 16880983]
20. Daniels R; Vanderleyden J; Michiels J. Quorum Sensing and Swarming Migration in Bacteria. FEMS Microbiol. Rev2004, 28, 261–289. [PubMed: 15449604]
21. Davies DG; Parsek MR; Pearson JP; Iglewski BH; Costerton JW; Greenberg EPThe Involvement of Cell-to-Cell Signals in the Development of a Bacterial Biofilm. Science1998, 280, 295–298. [PubMed: 9535661]
22. de Kievit TRQuorum Sensing in Pseudomonas aeruginosa Biofilms. Environ. Microbiol2009, 11, 279–288. [PubMed: 19196266]
23. Reis RS; Pereira AG; Neves BC; Freire DMGGene Regulation of Rhamnolipid Production in Pseudomonas aeruginosa - A Review. Bioresour. Technol2011, 102, 6377–6384. [PubMed: 21498076]
24. Daniels R; Reynaert S; Hoekstra H; Verreth C; Janssens J; Braeken K; Fauvart M; Beullens S; Heusdens C; Lambrichts I; De Vos DE; Vanderleyden J; Vermant J; Michiels J. Quorum Signal Molecules as Biosurfactants Affecting Swarming in Rhizobium etli. Proc. Natl. Acad. Sci. U. S. A2006, 103, 14965–14970.
25. Davis BM; Richens JL; O'Shea P. Label-Free Critical Micelle Concentration Determination of Bacterial Quorum Sensing Molecules. Biophys. J2011, 101, 245–254. [PubMed: 21723835]
26. Gahan CG; Patel SJ; Boursier ME; Nyffeler KE; Jennings J; Abbott NL; Blackwell HE; Van Lehn RC; Lynn DMBacterial Quorum Sensing Signals Self-Assemble in Aqueous Media to Form Micelles and Vesicles: An Integrated Experimental and Molecular Dynamics Study. J. Phys. Chem. B2020, 124, 3616–3628. [PubMed: 32271573]
27. Jakubczyk D; Barth C; Kubas A; Anastassacos F; Koelsch P; Fink K; Schepers U; Brenner-Weiss G; Brase S. Deuterium-Labelled N-Acyl-L-Homoserine Lactones (AHLs)-Inter-Kingdom Signalling Molecules-Synthesis, Structural Studies, and Interactions with Model Lipid Membranes. Anal. Bioanal. Chem2012, 403, 473–482. [PubMed: 22367286]
28. Barth C; Jakubczyk D; Kubas A; Anastassacos F; Brenner-Weiss G; Fink K; Schepers U; Brase S; Koelsch P. Interkingdom Signaling: Integration, Conformation, and Orientation of N-Acyl-L-Homoserine Lactones in Supported Lipid Bilayers. Langmuir2012, 28, 8456–8462. [PubMed: 22568488]
29. Toyofuku M; Morinaga K; Hashimoto Y; Uhl J; Shimamura H; Inaba H; Schmitt-Kopplin P; Eberl L; Nomura N. Membrane Vesicle-Mediated Bacterial Communication. ISME J. 2017, 11, 1504–1509. [PubMed: 28282039]
30. Davis BM; Jensen R; Williams P; O'Shea P. The Interaction of N-Acylhomoserine Lactone Quorum Sensing Signaling Molecules with Biological Membranes: Implications for Inter-Kingdom Signaling. PLoS One2010, 5, e13522.
31. Song DK; Meng JC; Cheng J; Fan Z; Chen PY; Ruan HF; Tu ZY; Kang N; Li N; Xu Y; Wang XB; Shi F; Mu LB; Li TF; Ren WR; Lin X; Zhu J; Fang XH; Amrein MW; Wu WH; Yan LT; Lu JH; Xia T; Shi Y. Pseudomonas aeruginosa Quorum-Sensing Metabolite Induces Host Immune Cell Death through Cell Surface Lipid Domain Dissolution. Nat. Microbiol2019, 4, 97–111. [PubMed: 30510173]
32. Lentini R; Martin NY; Forlin M; Belmonte L; Fontana J; Cornella M; Martini L; Tamburini S; Bentley WE; Jousson O; Mansy SSTwo-Way Chemical Communication between Artificial and Natural Cells. ACS Cent. Sci2017, 3, 117–123. [PubMed: 28280778]
33. Hughes DT; Sperandio V. Inter-Kingdom Signalling: Communication Between Bacteria and Their Hosts. Nat. Rev. Microbiol2008, 6, 111–120. [PubMed: 18197168]
34. Kravchenko VV; Kaufmann GF; Mathison JC; Scott DA; Katz AZ; Grauer DC; Lehmann M; Meijler MM; Janda KD; Ulevitch RJModulation of Gene Expression via Disruption of NF-Kappa B Signaling by a Bacterial Small Molecule. Science2008, 321, 259–263. [PubMed: 18566250]
35. Zhou J; Loftus AL; Mulley G; Jenkins ATAA Thin Film Detection/Response System for Pathogenic Bacteria. J. Am. Chem. Soc2010, 132, 6566–6570. [PubMed: 20405918]

36. Yates EA; Philipp B; Buckley C; Atkinson S; Chhabra SR; Sockett RE; Goldner M; Dessaux Y; Camara M; Smith H; Williams P. N-Acylhomoserine Lactones Undergo Lactonolysis in a pH-, Temperature-, and Acyl Chain Length-Dependent Manner During Growth of Yersinia pseudotuberculosis and Pseudomonas aeruginosa. Infect. Immun2002, 70, 5635–5646. [PubMed: 12228292]
37. Yoon BK; Jackman JA; Kim MC; Cho NJSpectrum of Membrane Morphological Responses to Antibacterial Fatty Acids and Related Surfactants. Langmuir2015, 31, 10223–10232.
38. Hodgkinson JT; Galloway W; Casoli M; Keane H; Su XB; Salmond GPC; Welch M; Spring DRRobust Routes for the Synthesis of N-Acylated-L-Homoserine Lactone (AHL) Quorum Sensing Molecules with High Levels of Enantiomeric Purity. Tetrahedron Lett. 2011, 52, 3291–3294.
39. Holloway BWGenetic Recombination in Pseudomonas aeruginosa. J. Gen. Microbiol1955, 13, 572–581. [PubMed: 13278508]
40. Jacobs MA; Alwood A; Thaipisuttikul I; Spencer D; Haugen E; Ernst S; Will O; Kaul R; Raymond C; Levy R; Liu CR; Guenthner D; Bovee D; Olson MV; Manoil C. Comprehensive Transposon Mutant Library of Pseudomonas aeruginosa. Proc. Natl. Acad. Sci. U. S. A2003, 100, 14339–14344.
41. Mayer LD; Hope MJ; Cullis PRVesicles of Variable Sizes Produced by a Rapid Extrusion Procedure. Biochim. Biophys. Acta1986, 858, 161–168. [PubMed: 3707960]
42. Lapinski MM; Castro-Forero A; Greiner AJ; Ofoli RY; Blanchard GJComparison of Liposomes Formed by Sonication and Extrusion: Rotational and Translational Diffusion of an Embedded Chromophore. Langmuir2007, 23, 11677–11683.
43. Lee MR; Raman N; Ortiz-Bermudez P; Lynn DM; Palecek SP14-Helical Beta-Peptides Elicit Toxicity against C. albicans by Forming Pores in the Cell Membrane and Subsequently Disrupting Intracellular Organelles. Cell Chem. Biol2019, 26, 289–299. [PubMed: 30581136]
44. Moga A; Yandrapalli N; Dimova R; Robinson T. Optimization of the Inverted Emulsion Method for High-Yield Production of Biomimetic Giant Unilamellar Vesicles. ChemBioChem2019, 20, 2674–2682. [PubMed: 31529570]
45. Cremer PS; Boxer SGFormation and Spreading of Lipid Bilayers on Planar Glass Supports. J. Phys. Chem. B1999, 103, 2554–2559.
46. Kolahdouzan K; Jackman JA; Yoon BK; Kim MC; Johal MS; Cho NJOptimizing the Formation of Supported Lipid Bilayers from Bicellar Mixtures. Langmuir2017, 33, 5052–5064. [PubMed: 28457139]
47. Smith TJ; Wang CX; Abbott NLRedox-Triggered Mixing and Demixing of Surfactants within Assemblies Formed in Solution and at Surfaces. J. Colloid Interface Sci2017, 502, 122–133. [PubMed: 28478219]
48. Lichtenberg D; Ahyayauch H; Alonso A; Goni FMDetergent Solubilization of Lipid Bilayers: A Balance of Driving Forces. Trends Biochem. Sci2013, 38, 85–93. [PubMed: 23290685]
49. Roux B. The Calculation of the Potential of Mean Force Using Computer-Simulations. Comput Phys Commun1995, 91, 275–282.
50. Best RB; Zhu X; Shim J; Lopes PEM; Mittal J; Feig M; MacKerell ADOptimization of the Additive Charmm All-Atom Protein Force Field Targeting Improved Sampling of the Backbone Phi, Psi and Side-Chain Chi(1) and Chi(2) Dihedral Angles. J Chem Theory Comput2012, 8, 3257–3273. [PubMed: 23341755]
51. Jo S; Kim T; Iyer VG; Im W. Charmm-Gui: A Web-Based Graphical User Interface for CHARMM. J. Comput. Chem2008, 29, 1859–1865. [PubMed: 18351591]
52. Kim S; Lee J; Jo S; Brooks CL; Lee HS; Im W. Charmm-Gui Ligand Reader and Modeler for CHARMM Force Field Generation of Small Molecules. J. Comput. Chem2017, 38, 1879–1886. [PubMed: 28497616]
53. Pronk S; Pall S; Schulz R; Larsson P; Bjelkmar P; Apostolov R; Shirts MR; Smith JC; Kasson PM; van der Spoel D; Hess B; Lindahl E. Gromacs 4.5: A High-Throughput and Highly Parallel Open Source Molecular Simulation Toolkit. Bioinformatics2013, 29, 845–854. [PubMed: 23407358]

54. Hub JS; de Groot BL; van der Spoel DGWham- A Free Weighted Histogram Analysis Implementation Including Robust Error and Autocorrelation Estimates. J Chem Theory Comput2010, 6, 3713–3720.
55. Rumbaugh KP; Griswold JA; Hamood ANThe Role of Quorum Sensing in the in vivo Virulence of Pseudomonas aeruginosa. Microbes Infect. 2000, 2, 1721–1731. [PubMed: 11137045]
56. Gooderham WJ; Hancock REWRegulation of Virulence and Antibiotic Resistance by Two-Component Regulatory Systems in Pseudomonas aeruginosa. FEMS Microbiol. Rev2009, 33, 279–294. [PubMed: 19243444]
57. Coggan KA; Wolfgang MCGlobal Regulatory Pathways and Cross-Talk Control Pseudomonas aeruginosa Environmental Lifestyle and Virulence Phenotype. Curr. Issues Mol. Biol2012, 14, 47–69. [PubMed: 22354680]
58. Crone S; Vives-Florez M; Kvich L; Saunders AM; Malone M; Nicolaisen MH; Martinez-Garcia E; Rojas-Acosta C; Gomez-Puerto MC; Calum H; Whiteley M; Kolter R; Bjarnsholt T. The Environmental Occurrence of Pseudomonas aeruginosa. APMIS2020, 128, 220–231. [PubMed: 31709616]
59. Reviakine I; Johannsmann D; Richter RPHearing What You Cannot See and Visualizing What You Hear: Interpreting Quartz Crystal Microbalance Data from Solvated Interfaces. Anal. Chem2011, 83, 8838–8848. [PubMed: 21939220]
60. Thid D; Benkoski JJ; Svedhem S; Kasemo B; Gold J. Dha-Induced Changes of Supported Lipid Membrane Morphology. Langmuir2007, 23, 5878–5881. [PubMed: 17455967]
61. Tabaei SR; Choi JH; Zan GH; Zhdanov VP; Cho NJSolvent-Assisted Lipid Bilayer Formation on Silicon Dioxide and Gold. Langmuir2014, 30, 10363–10373.
62. Ulrich AS; Sami M; Watts A. Hydration of DOPC Bilayers by Differential Scanning Calorimetry. Biochim. Biophys. Acta-Biomembr1994, 1191, 225–230.
63. Yoon BK; Jackman JA; Kim MC; Sut TN; Cho NJCorrelating Membrane Morphological Responses with Micellar Aggregation Behavior of Capric Acid and Monocaprin. Langmuir2017, 33, 2750–2759. [PubMed: 28263610]
64. Yoon BK; Jackman JA; Park S; Mokrzecka N; Cho NJCharacterizing the Membrane-Disruptive Behavior of Dodecylglycerol Using Supported Lipid Bilayers. Langmuir2019, 35, 3568–3575. [PubMed: 30720282]
65. Yoon BK; Park S; Jackman JA; Cho NJSupported Lipid Bilayer Platform for Characterizing the Optimization of Mixed Nano-Micelles. Appl. Mater. Today2020, 19, 100598.
66. Ortiz BJ; Boursier ME; Barrett KL; Manson DE; Amador-Noguez D; Abbott NL; Blackwell HE; Lynn DMLiquid Crystal Emulsions That Intercept and Report on Bacterial Quorum Sensing. ACS Appl. Mater. Interfaces2020, 12, 29056–29065.
67. Laabei M; Jamieson WD; Lewis SE; Diggle SP; Jenkins ATAA New Assay for Rhamnolipid Detection-Important Virulence Factors of Pseudomonas aeruginosa. Appl. Microbiol. Biotechnol2014, 98, 7199–7209. [PubMed: 24974281]
68. Come B; Donato M; Potenza LF; Mariani P; Itri R; Spinozzi F. The Intriguing Role of Rhamnolipids on Plasma Membrane Remodelling: From Lipid Rafts to Membrane Budding. J. Colloid Interface Sci2021, 582, 669–677. [PubMed: 32916572]
69. Glansdorp FG; Thomas GL; Lee JJK; Dutton JM; Salmond GPC; Welch M; Spring DRSynthesis and Stability of Small Molecule Probes for Pseudomonas aeruginosa Quorum Sensing Modulation. Org. Biomol. Chem2004, 2, 3329–3336. [PubMed: 15534711]
70. Boursier ME; Combs JB; Blackwell HEN-Acyl L-Homocysteine Thiolactones Are Potent and Stable Synthetic Modulators of the Rhlr Quorum Sensing Receptor in Pseudomonas aeruginosa. ACS Chemical Biology2019, 14, 186–191. [PubMed: 30668907]
71. Charlton TS; de Nys R; Netting A; Kumar N; Hentzer M; Givskov M; Kjelleberg S. A Novel and Sensitive Method for the Quantification of N-3-Oxoacyl Homoserine Lactones Using Gas Chromatography-Mass Spectrometry: Application Ito a Model Bacterial Biofilm. Environ. Microbiol2000, 2, 530–541. [PubMed: 11233161]
72. Kim MC; Gunnarsson A; Tabaei SR; Hook F; Cho NJSupported Lipid Bilayer Repair Mediated by Ah Peptide. Phys. Chem. Chem. Phys2016, 18, 3040–3047. [PubMed: 26739239]
73. Dimova R; Marques CM, The Giant Vesicle Book. 1 ed.; CRC Press: Boca Raton, 2019; pp 1–676.

74. Jin T; Patel SJ; Van Lehn RCMolecular Simulations of Lipid Membrane Partitioning and Translocation by Bacterial Quorum Sensing Modulators. PLoS One2021, 16, e0246187.

75. Abdel-Mawgoud AM; Lepine F; Deziel E. Rhamnolipids: Diversity of Structures, Microbial Origins and Roles. Appl. Microbiol. Biotechnol2010, 86, 1323–1336. [PubMed: 20336292]

76. Yoon BK; Park S; Ma GJ; Kolahdouzan K; Zhdanov VP; Jackman JA; Cho NJCompeting Interactions of Fatty Acids and Monoglycerides Trigger Synergistic Phospholipid Membrane Remodeling. J. Phys. Chem. Lett2020, 11, 4951–4957. [PubMed: 32478524]

77. Deziel E; Lepine F; Milot S; Villemur R. Rhla Is Required for the Production of a Novel Biosurfactant Promoting Swarming Motility in Pseudomonas aeruginosa: 3-(3-Hydroxyalkanoyloxy)Alkanoic Acids (HAAs), the Precursors of Rhamnolipids. Microbiology2003, 149, 2005–2013. [PubMed: 12904540]

78. Wang LH; Weng LX; Dong YH; Zhang LHSpecificity and Enzyme Kinetics of the Quorum-Quenching N-Acyl Homoserine Lactone Lactonase (AHL-Lactonase). J. Biol. Chem2004, 279, 13645–13651. [PubMed: 14734559]

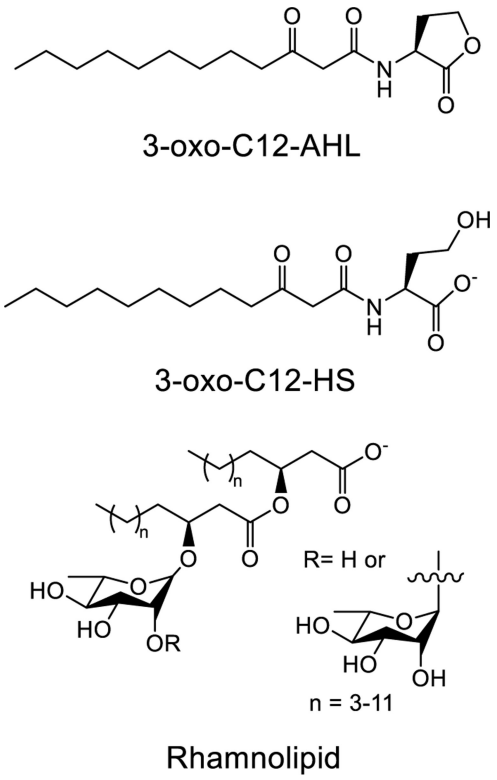

Figure 1:
Structures of the amphiphilic compounds examined experimentally and by molecular dynamics simulations in this study.

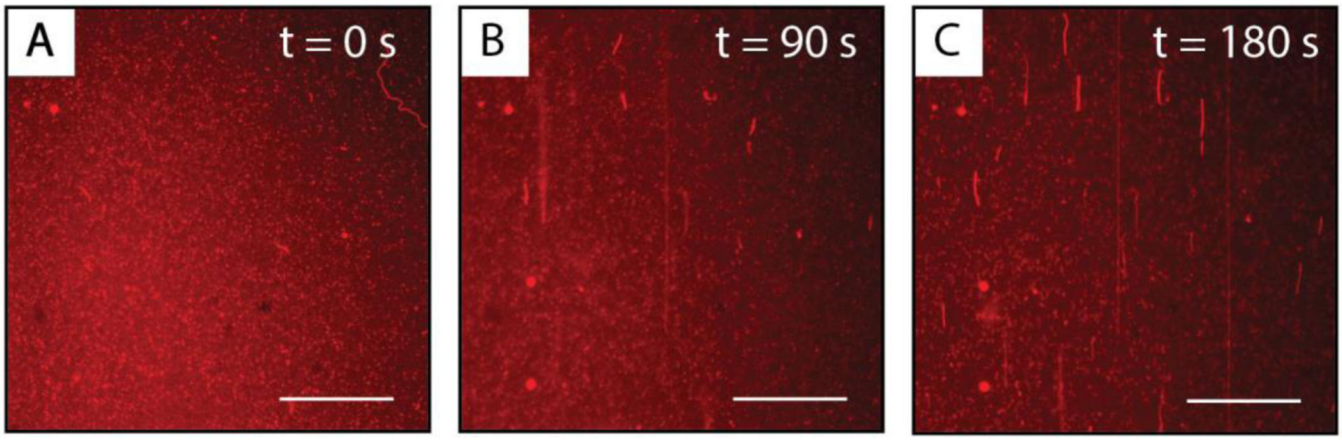

Figure 2:

Representative top-down fluorescence micrographs of structural reformations observed in fluorescently labeled DOPC SLBs after the introduction of cell-free supernatants of *P. aeruginosa* cultures grown for 24 hours. The micrographs were acquired (A) 0 seconds, (B) 90 seconds, and (C) 180 seconds after the first membrane reformations were observed on the surface of the bilayer. The direction of flow in all the images is from the bottom to the top of the image. Scale bars are 30 μm.

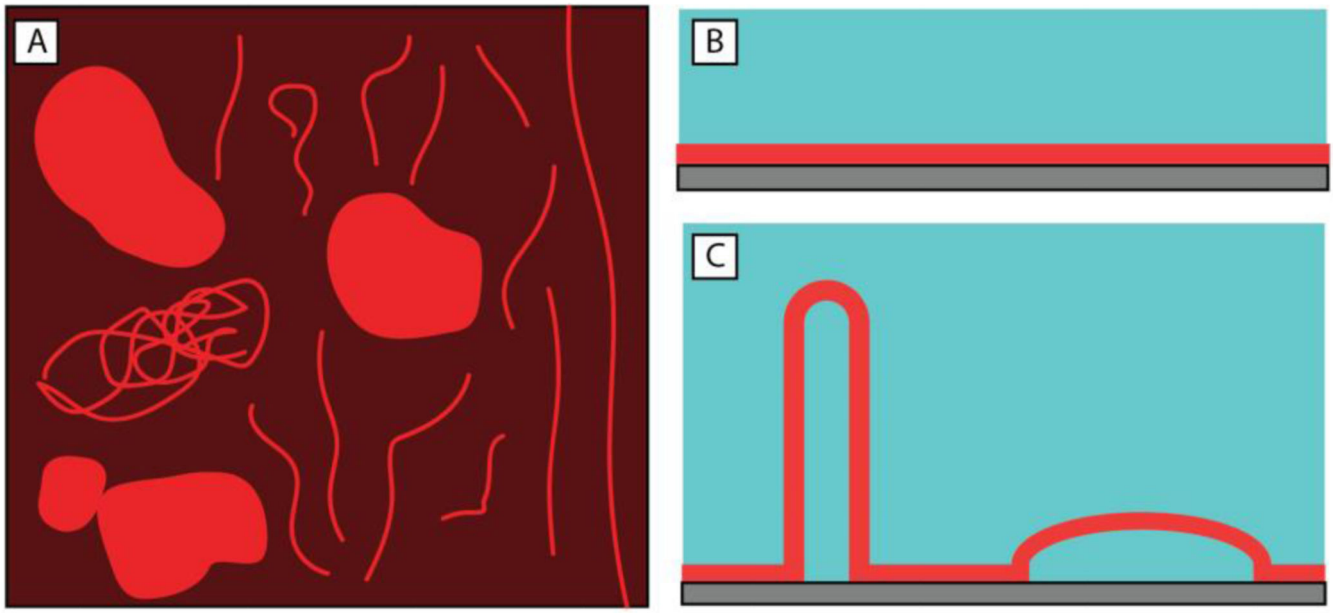

Figure 3:
Illustrations depicting membrane reformations (microtubules and hemispherical caps) observed in our experiments and in past studies of interactions of natural and synthetic amphiphiles in contact with SLBs.[37] (A) Top-down depiction of a remodeled bilayer showing both long and short tubule structures and hemispherical caps. (B,C) Side view of (B) a SLB without any structural reformations and (C) a SLB with both (left) extended microtubules and (right) hemispherical caps after membrane reformation.

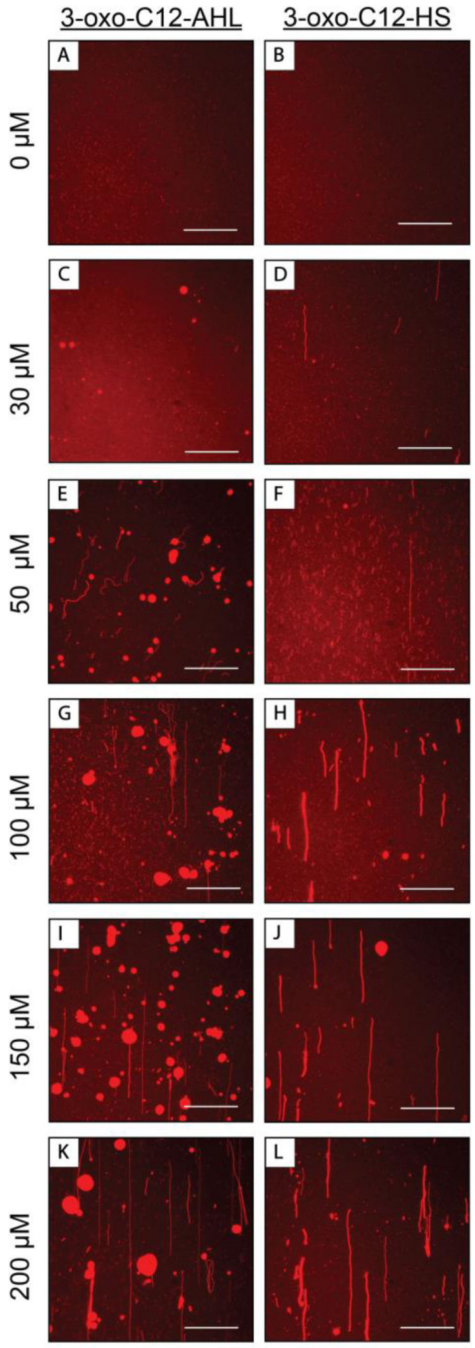

Figure 4:

Representative top-down fluorescence micrographs of fluorescently labeled DOPC SLBs that are either (A, B) stable under a continuous flow of buffer or (C-L) have undergone structural reformations after interacting with a continuous flow of (*left images*: C, E, G, I, K) 3-oxo-C12-AHL or (*right images*: D, F, H, J, L) 3-oxo-C12-HS solutions. Images were acquired 360 seconds after the onset of membrane restructuring. The concentration of amphiphiles used in each experiment were (C,D) 30 μM, (E,F) 50 μM, (G,H) 100 μM, (I,J)

150 μM, or (K,L) 200 μM. The direction of flow in all images was from the bottom to the top of the image. Scale bars are 30 μm.

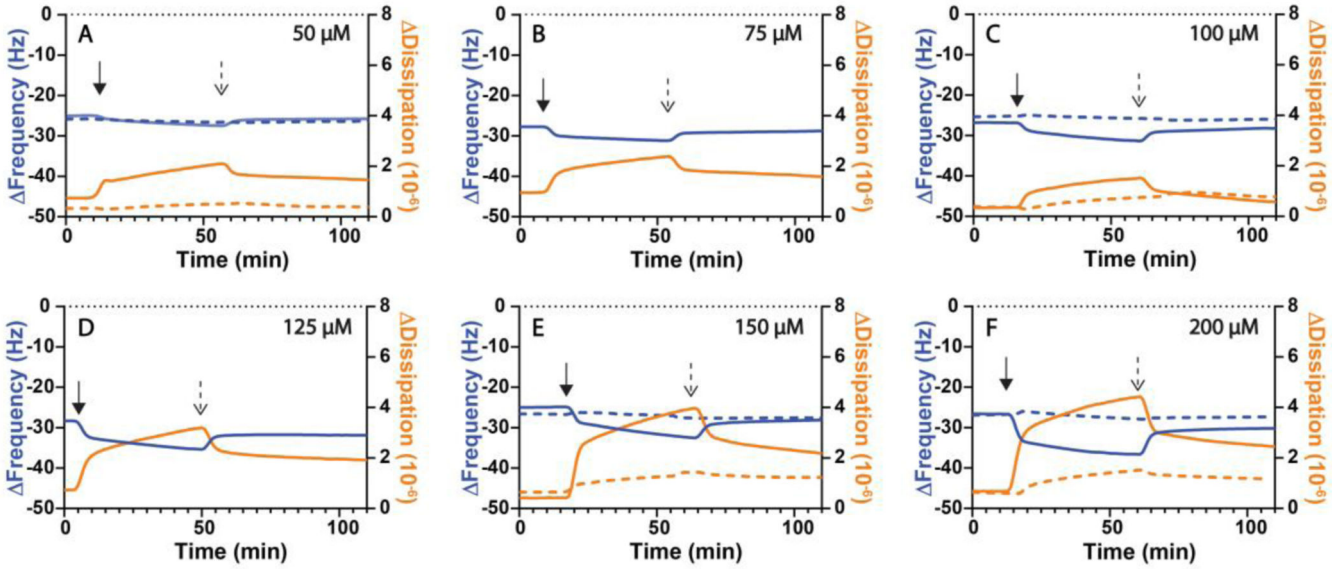

Figure 5:

Representative QCM-D measurements of large-scale bilayer reformations in DOPC SLBs initiated by the introduction of (solid lines) 3-oxo-C12-AHL or (dashed lines) 3-oxo-C12-HS solutions at (A) 50 μM, (B) 75 μM, (C) 100 μM, (D) 125 μM, (E) 150 μM, (F) 200 μM. The changes in frequency (ΔFrequency, blue lines; referred to as Δf in the main text for brevity), and dissipation (ΔDissipation, orange lines; referred to as ΔD in the main text for brevity) shown are representative of three or four independent experiments. The initial measurement values (t=0 min) of these experiments correspond to a DOPC SLB on an SiO_2 surface. Either 3-oxo-C12-AHL or 3-oxo-C12-HS solutions were introduced to the bilayer at the time indicated by the solid arrow and a buffer wash was introduced at the time indicated by the dashed arrow.

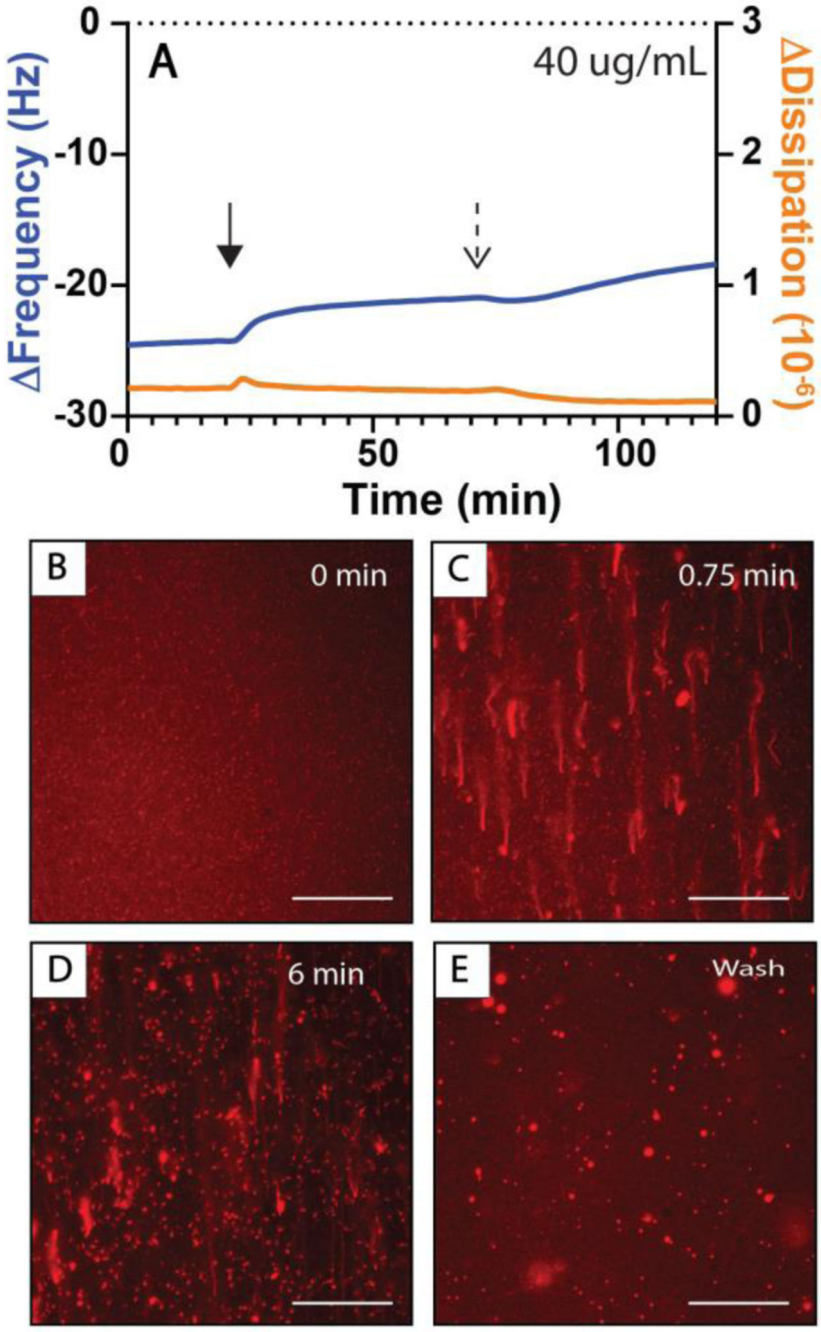

Figure 6:

Measurements of membrane restructuring occurring in DOPC SLBs introduced to 40 μg/mL solutions of rhamnolipid. (A) QCM-D measurements of bilayer reformations initiated by the introduction of rhamnolipid solutions with changes in frequency (ΔFrequency, blue lines; referred to as Δf in the main text for brevity), and dissipation (ΔDissipation, orange lines; referred to as ΔD in the main text for brevity) shown are representative of three or four independent experiments. The initial measurement values (t=0 min) of these experiments correspond to a DOPC SLB on an SiO_2 surface. Rhamnolipid solutions were introduced to

the bilayer at the time indicated by the solid arrow and the buffer was introduced at the time indicated by the dashed arrow. (B-E) fluorescence micrographs of bilayer restructuring occurring at (B) 0 sec, (C) 45 sec, and (D) 6 min after the first bilayer restructuring events had been observed or (E) after at least 8 minutes of washing the bilayer with buffer. The direction of flow in all images is from the bottom to the top of the image. Scale bars are 30 μm.

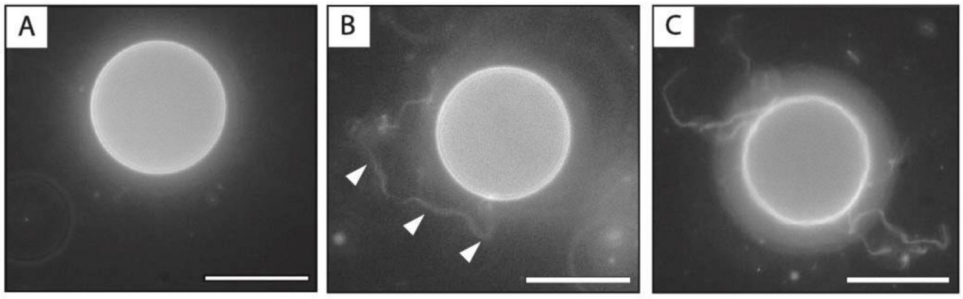

D

Condition	Percent Outer Tubulation
Buffer	4 ± 4%
3-oxo-C12-AHL (100 μM)	82 ± 7%
Rhamnolipid (25 μg/mL)	100 ± 0%

Figure 7:

(A-C) Fluorescence microscopy images of DOPC GUVs (A) in buffer or (B,C) after being introduced to (B) 100 μM 3-oxo-C12-AHL or (C) 25 μg/mL rhamnolipid. The white arrowheads in (B) point to external tubules formed after incubation with 3-oxo-C12-AHL. (D) Percentage of vesicles observed to show signs of outer tubulation (see text) upon the addition of 3-oxo-C12-AHL, rhamnolipid, or buffer as a control. The value shown is the average and standard deviation of three (n=3) independent samples.

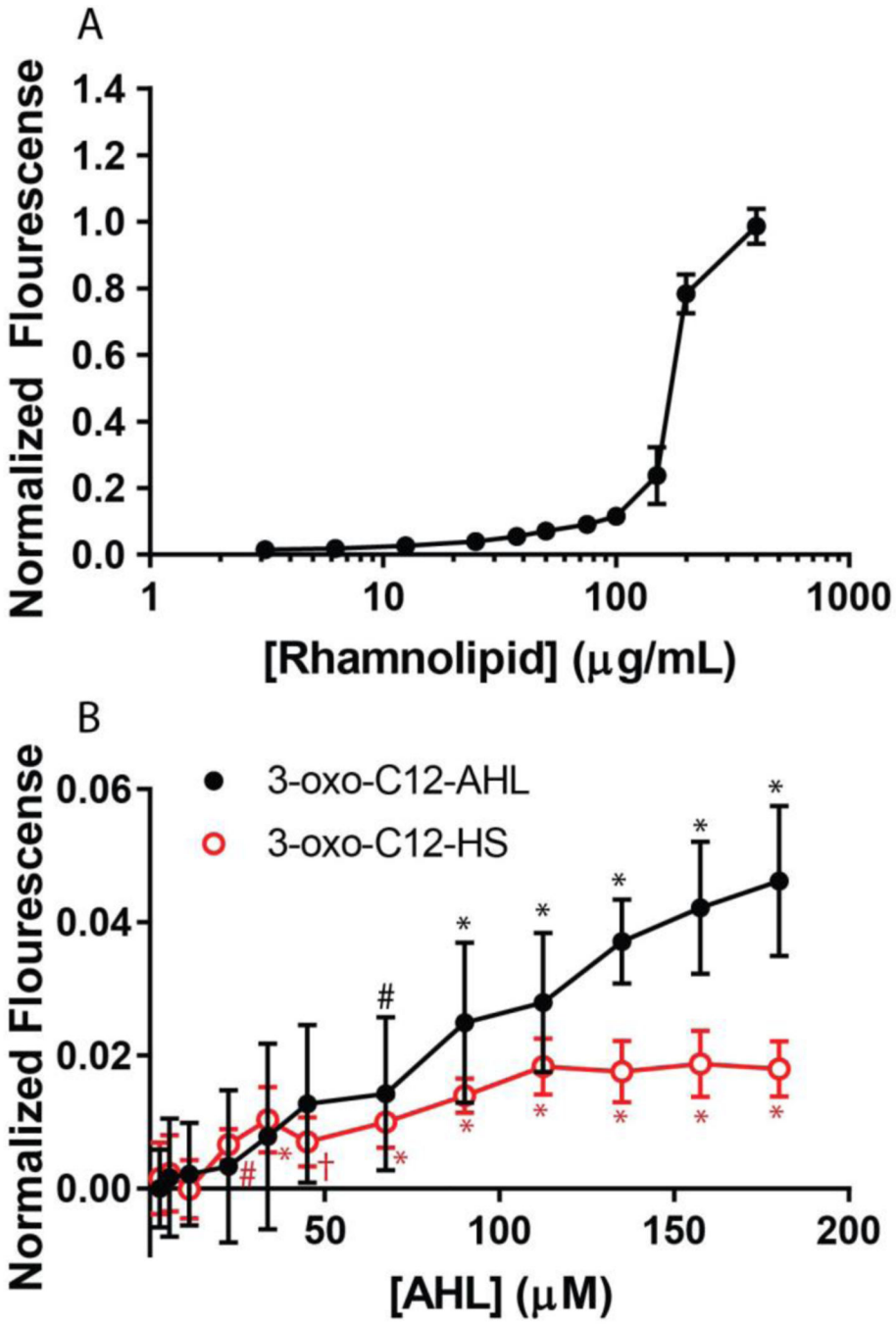

Figure 8:

Normalized calcein fluorescence intensity values of (A) rhamnolipid and (B) 3-oxo-C12-AHL (black circles) and 3-oxo-C12-HS (red squares) at various concentrations interacting with 100 μM of calcein-loaded DOPC vesicles. Statistical significance compared to a buffer control is indicated for concentrations of 3-oxo-C12-AHL (black asterisks) and 3-oxo-C12-HS (red asterisks), with the following p values: $^{\#}p<0.05$, $^{\dagger}p<0.01$, $^{*}p<0.0001$. All points shown are the average and standard deviation of nine independent fluorescence

measurements (see Materials and Methods). For the rhamnolipid measurements, some error bars are obscured by the size of the data point.

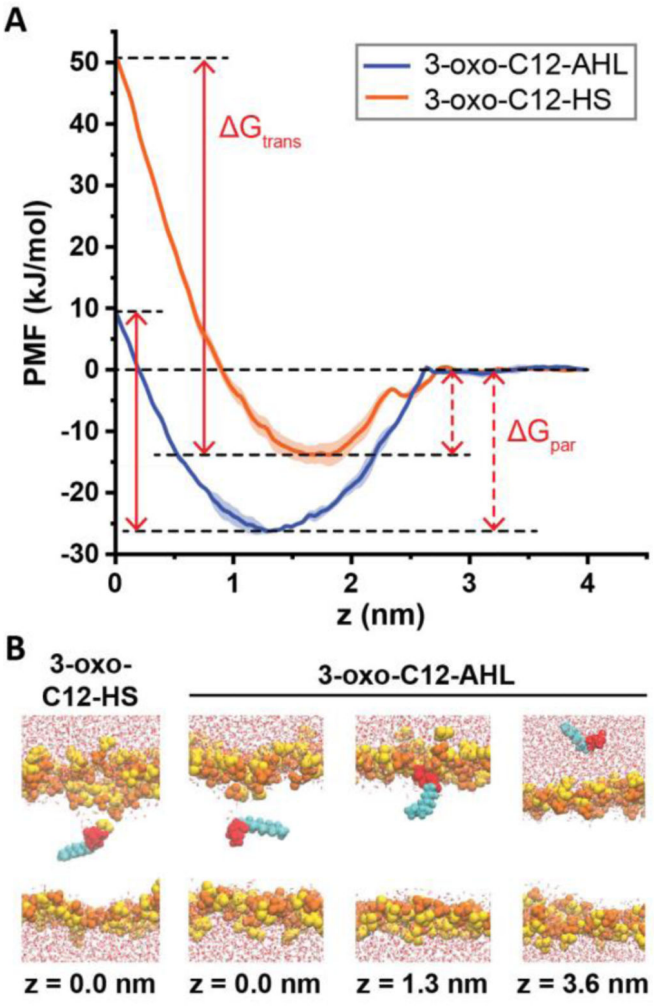

C

Molecule	ΔG_{par} (kJ/mol)	ΔG_{trans} (kJ/mol)
3-oxo-C12-AHL	-26.29 ± 0.32	35.57 ± 0.45
3-oxo-C12-HS	-13.87 ± 1.43	67.59 ± 4.15
rha-C10-C10	-16.55 ± 3.80	56.90 ± 4.53
rha-rha-C10-C10	-31.99 ± 0.15	62.68 ± 4.18
GML	-34.34 ± 0.96	22.70 ± 0.96
Lauric Acid	-21.71 ± 3.61	43.97 ± 4.77

Figure 9:

Results of molecular dynamics simulations. (A) Potentials of mean force (PMFs) of 3-oxo-C12-AHL (blue) and 3-oxo-C12-HS (orange) as a function of the distance along the DOPC bilayer normal (z). The midplane of the membrane is at z = 0 nm and the PMF is set to zero at $z = 4$ nm. Each curve shows the average of two independent PMFs and error bars show the standard deviation. The plots also illustrate the definition of ΔG_{par} as the free energy difference between the PMF minimum and the value in solution and ΔG_{trans} as the free energy difference between the PMF minimum and maximum. (B) Snapshots showing

configurations of AHLs and bilayers for different characteristic values of z in the PMF of 3-oxo-C12-AHL. A snapshot for z = 0 nm for 3-oxo-C12-HS is shown to highlight the local bilayer disruption that contributes to the larger value of ΔG_{trans}. Lipid head groups are yellow/orange, AHL heads are red, AHL tail groups are cyan, and water is drawn as red and white. Lipid tail groups are not shown for clarity. (C) Table showing ΔG_{par} and ΔG_{trans} values for all molecules simulated here.

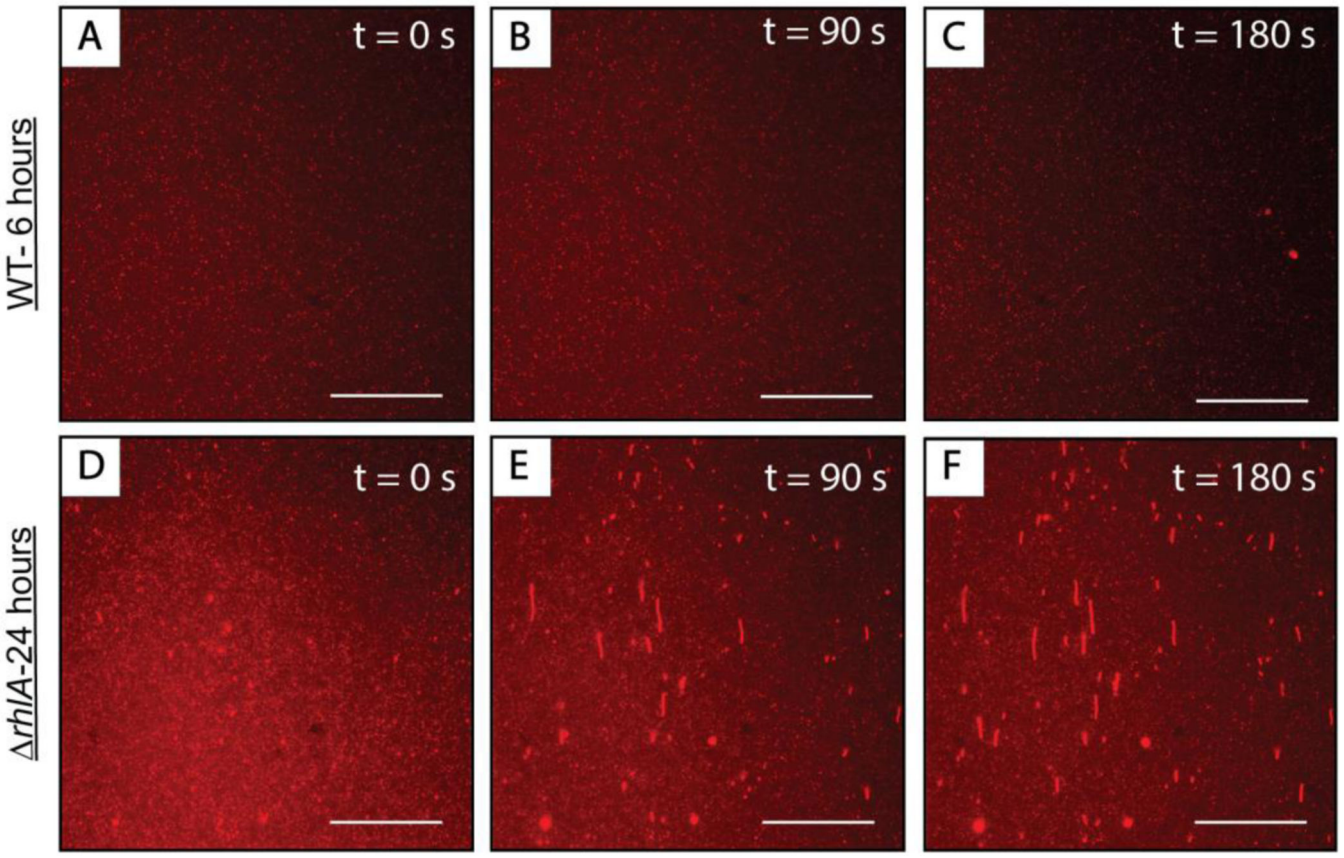

Figure 10:

Representative top-down fluorescence micrographs of structural reformations occurring in fluorescently labeled DOPC SLBs after the introduction of cell-free supernatants of (A-C) wild type *P. aeruginosa* cultures grown for 6 hours or (D-F) mutant strain Δ*rhlA P. aeruginosa* cultures grown for 24 hours. The micrographs were acquired at (A, D) 0 seconds, (B, E) 90 seconds, and (C, F) 180 seconds after the first membrane reformations were observed on the surface of the bilayer. The direction of flow in all the images is from the bottom to the top of the screen. Scale bars are 30 μm.